Journal of Environmental Management 326 (2023) 116819

Contents lists available at ScienceDirect

Journal of Environmental Management

journal homepage: www.elsevier.com/locate/jenvman

Research article

Combined organic coagulants and photocatalytic processes for winery wastewater treatment

Nuno Jorge [a,b,*], Ana R. Teixeira [b], Marco S. Lucas [b], José A. Peres [b]

[a] Escuela Internacional de Doctorado (EIDO), Campus da Auga, Campus Universitário de Ourense, Universidade de Vigo, As Lagoas, 32004, Ourense, Spain
[b] Centro de Química de Vila Real (CQVR), Departamento de Química, Universidade de Trás-os-Montes e Alto Douro (UTAD), Quinta de Prados, 5001-801, Vila Real, Portugal

ARTICLE INFO

Keywords:
Coagulation-flocculation-decantation
Natural organic coagulants
Potassium persulfate
Photo-fenton

ABSTRACT

Due to the consumers demand for quality wines, washing and disinfection operations are necessary in wine productions, leading to the generation of large volumes of winery wastewater (WW) with a high organic content which has the potential to cause irreversible environmental impacts. The aim and novelty of this work is the production of natural organic coagulants (NOCs) to be applied in coagulation-flocculation-decantation (CFD) process. To complement this treatment process, it is also aimed the performed a photo-Fenton process, combining hydrogen peroxide (H_2O_2) and potassium persulfate (KPS). The Fourier-transform infrared spectroscopy (FTIR) and scanning electron microscope (SEM) showed that NOCs are carbon-based materials with adsorption capacity. Under the best operational conditions, NOCs achieved a turbidity removal between 86.2 and 98.9%, a total suspended solids (TSS) removal ranging between 85.0 and 94.9% and a dissolved organic carbon (DOC) removal ranging between 14.1 and 44.9%. To degrade the DOC present in the WW, different advanced oxidation processes (AOPs) were tested. Results showed that KPS-photo-Fenton, under the best operational conditions [Fe^{2+}] = 2.5 mM, [KPS] = 1.0 mM, pH = 3.0, radiation UV-C mercury lamp (254 nm), agitation 350 rpm, temperature 298 K, reaction time 240 min achieved a DOC removal of 91.2 and 96.8%, with a H_2O_2 consumption of 156.9 and 199.0 mM, respectively for red and white WW. With application of combined CFD-KPS-photo-Fenton process, it was observed an increase of DOC removal with lower H_2O_2 consumptions. The energy consumption of the photosystem was evaluated by application of electric energy per mass (E_{EM}). The application of KPS-photo-Fenton process achieved an E_{EM} of 0.308 and 0.0309 kWh/g/L DOC, with a cost of 2.05 and 2.59 €/g/L DOC respectively for red and white WW. The combination of CFD-KPS-photo-Fenton decreased significantly the costs of treatment and the treated wastewater achieved the Portuguese legal values for wastewater discharge. This work shows that NOCs are a promising technology that can be an alternative to traditional metal salts, the combination of sulfate radicals with hydroxyl radicals can achieve high DOC removal and the combination of CFD with KPS-photo-Fenton process can decrease the operational costs.

1. Introduction

The production of wine is one of the largest industries in the world. To maintain the quality of the product required by the consumers, various washing operations are necessary to be performed during the crushing and pressing of grapes as well as rinsing of fermentation tanks, barrels and other equipment or surfaces, and therefore, wineries, distilleries and other grape processing industries annually generate a large volume of wastewater (Malandra et al., 2003) with a pH ranging between 3 and 4, a chemical oxygen demand (COD) between 800 and 25, 000 mg O_2/L (Petruccioli et al., 2002), high organic load of soluble sugars, organic acids, alcohols, polyphenols, tannins and structural polymers (Welz et al., 2016). Considering these values, the winery wastewater (WW) should not be directly conveyed to municipal wastewater treatment plants (WWTP) or released into the environment without proper treatment.

In this work, two processes are proposed to treat the WW, a physical-chemical process, namely coagulation-flocculation-decantation (CFD) process and a chemical process based in advanced oxidation processes (AOPs).

* Corresponding author. Escuela Internacional de Doctorado (EIDO), Campus da Auga, Campus Universitário de Ourense, Universidade de Vigo, As Lagoas, 32004, Ourense, Spain.
E-mail address: njorge@uvigo.es (N. Jorge).

https://doi.org/10.1016/j.jenvman.2022.116819
Received 16 August 2022; Received in revised form 14 November 2022; Accepted 15 November 2022
Available online 20 November 2022

The CFD process is an easy and cheap process that allows the separation of the solids suspended in the wastewater. Many authors share the use of hydrolysable metal salts as coagulants, however there are several risks associated to its use, such as dialysis encephalopathy and prevalence of Alzheimer's disease (Ghernaout et al., 2018). Therefore, more ecologic products should be applied to guarantee the safety of disposed water. Plants such as *Dactylis glomerata* L., *Daucus carota* L., *Festuca ampla Hack*. and *Tanacetum vulgare* L. are considered invasive plants and large quantities of herbicide, such as glyphosate, are spent every year to eradicate these plants. These herbicides can get over-accumulated in soils as residues and consequently become a biological and environmental concern (Cerdeira and Duke, 2006; Yin et al., 2008). In addition, after the vintage, large amounts of rachis without value for winemaking are disposed, thus it is a cheap subproduct that could be recycled, along with the invasive plants and be transformed as coagulants. In this direction, the application of invasive plants and agriculture subproducts as coagulants, and the recycling of wastewater for irrigation, two problems become one solution.

To degrade the organic matter dissolved in the wastewater, advanced oxidation processes (AOPs) can be applied. The AOPs refers to all treatment processes that work at near ambient temperature and pressure, involving the generation of hydroxyl radicals ($HO^{\bullet}$) with an oxidizing power of 2.80 V, which react immediately and non-selectively with most organic and organometallic pollutants until achieving total combustion or at least partial mineralization (Ganiyu et al., 2022). Depending on the type of oxidant used, AOPs can be designated HR-AOPs with the application of hydrogen peroxide (H_2O_2) or SR-AOPs, with the application of persulfate (PS) and peroxymonosulfate (PMS). Among the HR-AOPs, the Fenton process is the most common. In this process ferrous iron (Fe^{2+}) reacts with H_2O_2 to generate $HO^{\bullet}$ radicals (Equation (1)). The ferrous iron is oxidized in this reaction to ferric iron and a second process occurs (Fenton-like), in which the Fe^{3+} reacts with the H_2O_2 producing hydroperoxyl radicals ($HO_2^{\bullet}$) (Equation (2)). The Fe^{3+} reacts with the H_2O in solution, been reduced to Fe^{2+} (Equation (3)), however, this is a slow process (Lin et al., 2022).

$$Fe^{2+} + H_2O_2 \rightarrow Fe^{3+} + + HO^{\bullet} + HO^{-} \quad \text{Equation 1}$$

$$Fe^{3+} + H_2O_2 \rightarrow Fe^{2+} + HO_2^{\bullet} + H^{+} \quad \text{Equation 2}$$

$$Fe^{3+} + H_2O \rightarrow Fe^{2+} + HO^{\bullet} + H^{+} \quad \text{Equation 3}$$

The application of ultraviolet radiation (UV) to Fenton process is able to increase the efficiency of the reaction, due to the faster regeneration of Fe^{3+} to Fe^{2+} (Equation (4)) and at the same time, the production of $HO^{\bullet}$ radicals by photolysis of H_2O_2 (Equation (5)) (Jorge et al., 2022b; Khan et al., 2021).

$$Fe(HO)^{2+} + h\nu \rightarrow Fe^{2+} + HO^{\bullet} \quad \text{Equation 4}$$

$$H_2O_2 + h\nu \rightarrow 2HO^{\bullet} \quad \text{Equation 5}$$

In the last decade, the employment of sulfate radicals ($SO_4^{\bullet -}$) attracted a great attention on wastewater treatment applications (Shu et al., 2016), due to the high oxidizing potential (SO_4^{2-}; $E_{SO_4^{2-}} = 2.6$ V). The activation of persulfate is accomplished by various methods, such as heat or UV radiation (Equation (6)), transition metal (M^{n+}) (Equation (7)) or alkaline pH (Equation (8)) (Chen et al., 2016; Dbira et al., 2019; Huie et al., 1991; Rodríguez-Chueca et al., 2017), as follows:

$$S_2O_8^{2-} + heat\ or\ \text{UV} \rightarrow 2SO_4^{2-} \quad \text{Equation 6}$$

$$S_2O_8^{2-} + M^{n+} \rightarrow SO_4^{\bullet -} + M^{n+1} + SO_4^{2-} \quad \text{Equation 7}$$

$$SO_4^{\bullet -} + HO^{-} \rightarrow HO^{\bullet} + SO_4^{2-}\ (\text{at alkaline pH}) \quad \text{Equation 8}$$

The performance of oxidation process combining persulfate and hydrogen peroxide has been applied before on the treatment of trichloroethylene (Yan et al., 2013), chlorinated ethane (Ko et al., 2012), landfill leachate (Hilles et al., 2016), erythromycin (Li et al., 2017), and levofloxacin (Epold et al., 2015) due to the production of $SO_4^{\bullet -}$ and $HO^{\bullet}$ radicals simultaneously. However, most of these studies focus on the degradation of contaminants in distilled water, and these types of matrixes can't be compared to complex matrixes such as WW. In addition, to our knowledge, there is no information regarding the addition of both chemicals on the treatment of WW, and how both of them interact during oxidation process.

The main aim and major novelty of this work is the production and application of natural organic coagulants (NOC) to reduce the solid parts in the WW. It is also aimed in this work the application of an oxidation process combining hydrogen peroxide (H_2O_2) and persulfate (PS) to degrade the dissolved carbon and to evaluate the effect of CFD process in the efficiency of oxidation process. Finally, it is aimed in this work the study of the separation of wastewaters (red and white) for the oxidation of organic matter.

2. Material and methods

2.1. Reagents and winery wastewater sampling

Ferric chloride hexahydrate ($FeCl_3 \bullet 6H_2O$) and potassium peroxymonosulphate (PMS; $2KHSO_5 \bullet KHSO_4 \bullet K_2SO_4$) were supplied by Merck (Darmstadt, Germany), ferrous sulfate heptahydrate ($FeSO_4 \bullet 7H_2O$) was supplied by Panreac (Barcelona, Spain), potassium persulphate (KPS; $K_2S_2O_8$) was supplied by Scharlau (Barcelona, Spain), hydrogen peroxide (H_2O_2 30% w/w) and titanium(IV) oxysulfate solution 1.9–2.1%, were acquired by Sigma-Aldrich (Missouri, USA), sodium sulfite anhydrous (Na_2SO_3) was acquired by Labkem, Barcelona, Spain. For pH adjustment, it was used sodium hydroxide (NaOH) from Labkem (Barcelona, Spain) and sulphuric acid (H_2SO_4, 95%) from Scharlau, (Barcelona, Spain).

The winery wastewaters were collected from a cellar located in the north of Portugal. The samples were collected in plastic containers, transported to the laboratory and stored at −40 °C.

2.2. Analytical techniques

Different physical-chemical parameters were determined in order to characterize the WW, such as total suspended solids (TSS), chemical oxygen demand (COD), biological oxygen demand (BOD_5), total organic carbon (TOC) and total polyphenols (TPh). The main wastewater characteristics are shown in Table 1.

Total polyphenols (TPh) were measured by Folin-Ciocalteu method (Singleton and Rossi, 1965). Chemical oxygen demand (COD) analysis was carried out using a COD reactor from HACH Co. (Loveland, CO, USA) and a HACH DR 2400 spectrophotometer (Loveland, CO, USA) for colorimetric measurement. Biochemical oxygen demand (BOD_5) was determined using a respirometric OxiTop® IS 12 system (WTW, Yellow Springs, OH, USA). Dissolved organic carbon (DOC) samples were

Table 1
Winery wastewater characterization.

Parameters	Value	
Type of WW	Red	White
pH	4.0 ± 0.1	4.0 ± 0.1
Electrical conductivity (μS/cm)	62.5 ± 1.9	125 ± 3.8
Turbidity (NTU)	296 ± 8.9	203 ± 6.1
Total suspended solids – TSS (mg/L)	750 ± 22.5	453 ± 13.6
Chemical Oxygen Demand – COD (mg O_2/L)	2145 ± 64.4	1878 ± 56.3
Biochemical Oxygen Demand – BOD_5 (mg O_2/L)	550 ± 16.5	700 ± 21.0
Dissolved Organic Carbon – DOC (mg C/L)	400 ± 12.0	400 ± 12.0
Total polyphenols – TPh (mg gallic acid/L)	22.6 ± 0.7	16.4 ± 0.5
Iron (mg/L)	0.05 ± 0.002	0.05 ± 0.002
Biodegradability – BOD_5/COD	0.26 ± 0.008	0.37 ± 0.011

analyzed by direct injection of filtered samples into a Shimadzu TOC-L_{CSH} analyzer (Shimadzu, Kyoto, Japan), equipped with an ASI-L autosampler, and with an NDIR detector, the H_2O_2 concentration was determined using titanium (IV) oxysulfate (DIN 38 402H15 method) at 410 nm using a portable spectrophotometer from Hach (Loveland, Colorado, USA). The iron was analyzed by atomic absorption spectroscopy (AAS) using a Thermo Scientific™ iCE™ 3000 Series (Thermo Fisher Scientific, Massachusetts, USA). The turbidity was determined by a 2100 N IS Turbidimeter (Hach, Loveland, CO, USA), the TSS were determined by a portable spectrophotometer (Hach, Loveland, CO, USA), the pH was determined by a 3510 pH meter (Jenway, Cole-Parmer, UK) and conductivity was determined by a portable conductivity meter, VWR C030 (VWR, V. Nova de Gaia, Portugal), in accordance to the methodology of the Standard Methods (APHA et al., 1999).

The FTIR spectra of plant coagulants was obtained by mixing 2 mg of the plant powder with 200 mg KBr. The powder mixtures were then inserted into molds and pressed at 10 ton/cm^2 to obtain the transparent pellets. The samples were analyzed with an IRAffinity-1S Fourier Transform Infrared spectrometer (Shimadzu, Kyoto, Japan) and the infrared spectra in transmission mode were recorded in the 4000–400 cm^{-1} frequency region. The microstructural characterization was carried out with a scanning electron microscopy (FEI QUANTA 400 SEM/ESEM, Fei Quanta, Hillsboro, WA, USA). Mineral characterization (iron, copper, sodium, potassium, calcium and magnesium) was obtained by digestion of 500 mg of powder samples with nitric acid and hydrogen peroxide for 24 h. Then the samples were transferred to a Dry Block Heater reactor (Techne, Cole-Parmer, UK), at 60 °C. The temperature was gradually raised to 80 °C, 100 °C, 120 °C until reach 150 °C. The samples were cooled, and then a matrix solution (1.5 ml de HNO_3 p.a. conc. in 1000 mL distilled water) was added. Finally, the cations concentrations were analyzed by atomic absorption spectroscopy (AAS). The textural parameters of samples were obtained from N_2 adsorption–desorption isotherms at 77 K using a Micromeritics ASAP 2020 apparatus (TriStar II Plus, Micromeritics Instrument Corporation, Norcross, GA, USA). The samples were degassed at 150 °C up to 10^{-4} Torr before analysis. The specific surface area (S_{BET}) was determined by applying the Gurevitsch's rule at a relative pressure $p/p_0 = 0.30$ and according to the Brunauer, Emmett, Teller (BET) method from the linear part of the nitrogen adsorption isotherms. Different pore volumes were determined by the Barrett, Joyner, Halenda model (BJH model).

2.3. NOC preparation

All the plants used on this work were collected on the district of Vila Real, north of Portugal. The species *Daucus carota* L., *Dactylis glomerata* L., and *Festuca ampla Hack*. were collected at the GPS location 41°17′14.4″N 7°44′15.2″W. The species *Tanacetum vulgare* L. and *Vítis vinifera L.* were collected at the GPS location 41°18′25.2″N 7°42′06.2″W. On Table 2, it is indicated the plants sub-species, part collected for this study and the herbarium number attributed by UTAD for plant's identification.

Table 2
Plant identification, with description of specie, sub-specie, part collected and herbarium number.

Plant specie	Sub - specie	Part collected	Herbarium number
Dactylis glomerata L.	*lusitanica Stebbins et Zohary*	Seed	HVR22101
Daucus carota L.	*carota*	Seed	HVR22100
Festuca ampla Hack.	*ampla*	Seed	HVR22102
Tanacetum vulgare L.		Seed	HVR22099
Vitis vinifera L.		Stalk	

All the vegetable parts collected were washed and dried in an oven at 70 °C for 24 h. Them they were grounded into powder using a groundnut miller. The powder was then left to cool and stored in a tightly closed plastic jar.

2.4. Batch experiments

2.4.1. Coagulation-flocculation-decantation experimental set-up

The CFD experiments were performed in a conventional model Jar-Test apparatus (ISCO JF-4, Louisville, USA), using 500 mL of WW in 1000 mL beakers. In the CFD process, it was tested 5 NOCs (DG seeds, DC seeds, FA seeds, TV seeds and rachis and one metallic based coagulant (ferric chloride, 10% *w/w*). The CFD process was optimized as follows:

1) 0.1, 0.5, 1.0 and 2.0 g/L of coagulant were added to 500 mL of red WW samples at pH 3.0, 5.0, 7.0, 9.0 and 11.0, under the experimental conditions: fast mix 150 rpm/3 min, slow mix 20 rpm/20 min, temperature 298 K, sedimentation time 12 h. After the sedimentation, the supernatant was withdrawn from a point located 2 cm below the top of the liquid level of the beaker to determine the DOC, turbidity and TSS removal;
2) Pre-determined optimum values (pH and dosage) of NOC and ferric chloride obtained in (1) were added to the red WW samples. Then the stirring process (rpm/min) was varied under different fast mix – slow mix conditions (Table 3). After the sedimentation time, the supernatant was withdrawn to determine the DOC, turbidity and TSS removal.

2.4.2. Photocatalytic experimental set-up

The AOPs were performed in a cylindrical photoreactor with a volume of 500 mL. The reagents were added to the WW with a $DOC_0 = 400$ mg C/L, under constant agitation (350 rpm) at ambient temperature (298 K) with a reaction time of 240 min. For the reactions involving radiation, it was coupled to the reactor, a UV-C low pressure mercury vapor lamp (TNN 15/32) - working power = 15 W (795.8 W/m^2) and $\lambda_{max} = 254$ nm (*Heraeus*, Hanau, Germany). The oxidation process was performed, as follows:

1) Variation of different AOPs (H_2O_2, UV, UV + Fe^{2+}, H_2O_2+UV, Fenton and photo-Fenton) under the following conditions: pH = 3.0, $[Fe^{2+}] = 2.5$ mM;
2) Variation of wastewater pH (3.0–11.0) under the following experimental conditions: $[Fe^{2+}] = 2.5$ mM, radiation UV-C mercury lamp (254 nm);
3) Variation of Fe^{2+} concentration (0.5–5 mM) under the following experimental conditions: pH = 3.0, radiation UV-C mercury lamp (254 nm);
3) Variation of KPS and PMS concentrations (0.5–10 mM) in photo-Fenton oxidation, under the following experimental conditions: $[Fe^{2+}] = 2.5$ mM, pH = 3.0, radiation UV-C mercury lamp (254 nm);
4) Variation of treatment processes (photo-Fenton, KPS/H_2O_2/UV/Fe^{2+} and PMS/H_2O_2/UV/Fe^{2+}) for the treatment of white WW, under the experimental conditions: $[DOC]_0 = 400$ mg C/L, $[Fe^{2+}] = 2.5$ mM, [KPS] = [PMS] = 1.0 mM, pH = 3.0, radiation UV-C mercury lamp (254 nm).

Table 3
Mixing conditions applied on coagulation process.

Experiment	Fast mix rpm/min	Slow mix rpm/min	References
Mix 1	120/1	20/30	Amaral-Silva et al. (2016)
Mix 2	150/3	20/20	(Amor et al., 2012; Braz et al., 2010)
Mix 3	150/2	50/30	Ishak et al. (2018)
Mix 4	180/3	40/17	Marañón et al. (2015)
Mix 5	200/2	60/30	Amuda et al. (2006)

At the end of the experiments, sodium sulfite anhydrous was applied to quench the reactions. To determine the removal percentage of the parameters in study, it was applied Equation (9). Let X_i be defined as the removal of a given indicator (%) of water contamination (turbidity, TSS, DOC, COD and total polyphenols) that is achieved by a treatment (Peres et al., 2004):

$$X_i\ (\%) = \frac{C_0 - C_f}{C_0} * 100 \qquad \text{Equation 9}$$

where C_0 and C are the initial and final concentrations, respectively, of parameter i.

All the experiments were performed in triplicate and the observed standard deviation was always less than 5% of the reported values. Statistical analysis was performed with OriginLab 2019 software (Northampton, MA, USA).

3. Results and discussion

3.1. Coagulation-flocculation-decantation experiments

3.1.1. Characterization of NOCs

All the five NOCs were analyzed by FTIR to assess the nature of the active groups in the powder. By observation of Fig. 1, three bands were detected at 3444.9, 3390.9 and 3344.6 cm^{-1}, which could be attributed to the presence of hydroxyl groups (OH) present in the proteins, fatty acids, carbohydrates and lignin (Baptista et al., 2017; Kushwaha et al., 2014; Vunain et al., 2019). The band 2922.2 cm^{-1} could be attributed to C–H stretching of aliphatic structures assigned to fatty acids and lipids (Chung et al., 2018). The band 2848.9 cm^{-1} could be attributed to symmetric and asymmetric C–H vibration of methyl groups (Kushwaha et al., 2014) present on lipids, proteins (Chung et al., 2018), tannins and tannic acids (Prozil et al., 2014). The band 1741.7 cm^{-1} could be associated to the C═O stretching in ketones (*Vítis vinifera L.*) (Mageshkumar and Karthikeyan, 2016), and lipids (Zimmermann et al., 2017). The bands 1662.6 and 1518.0 cm^{-1} were associated to the presence of N–H bending and C–N stretching of amide I and amide II respectively, and proteins. The band 1425.4 cm^{-1} could be associated to O–H bending from cellulose. The band 1165.0 cm^{-1} could indicate the C–O stretching from polysaccharides (Rana et al., 2018). The band 1022.3 cm^{-1} indicated the C–O stretch which was an indication of the lignin structure (Kushwaha et al., 2014), or the presence of aliphatic amines with C═N type bond (Mageshkumar and Karthikeyan, 2016). The band 775.4 cm^{-1} could indicate the presence of N–H bending form proteins (Rana et al., 2018). It was also observed many peaks from 590.0 to 440.0 cm^{-1} which confirmed the presence of halogenated alkanes (Mageshkumar and Karthikeyan, 2016).

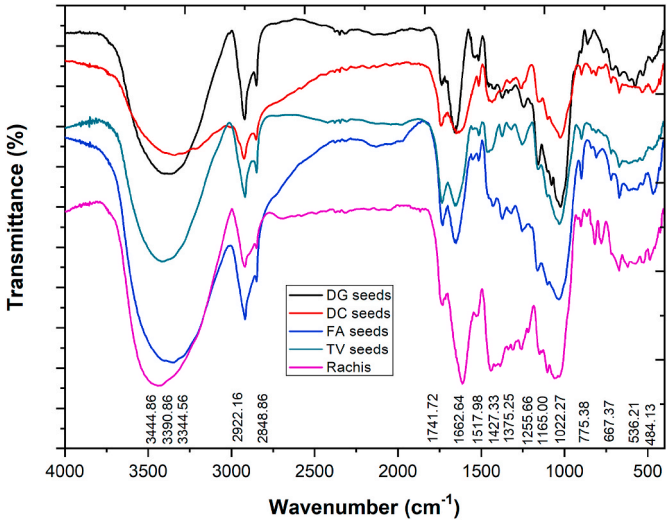

Fig. 1. FTIR spectrum of NOCs.

Fig. 2 shows the physical structure of the NOCs. It is observed that NOCs have a heterogeneous and disformed surface, with a porous morphology, which provides a lot of free spaces available, that can be important because they can facilitate the adsorption of particles with smaller size. It is also observed by the SEM images that NOCs present a chainlike a spherical structures, which are similar with the SEM images of *Moringa oleifera* seeds, observed in the work of Boulaadjoul et al. (2018).

The mineral composition of the NOCs was also studied. Iron and copper were observed to be the lowest minerals in NOCs constitution (Table 4), with a maximum of iron detected on DC seeds (6.3 mg/L) and a maximum of copper detected in DC seeds and rachis (1.2 mg/L). Regarding sodium, potassium, calcium and magnesium, it was observed on Table 4 high concentration levels on all NOCs. DC seeds were observed to have higher concentration of these minerals. Iwahashi et al. (1982) observed in studies performed on leaves, petioles and stems of cucumber plants, that during the plant's growth, the leaves lose most of these minerals. However, in petioles and stems the concentration remains almost the same during the stationary phase, which could explain the concentrations detected on the seeds and rachis.

The specific surface area and pore characteristics of NOCs are shown in Table 5. These results showed that all NOCs had a small specific surface area, ranging from 0.00 to 0.45 m^2/g, which indicates that NOCs are organic materials without mesoporosity. The shape of its N_2 adsorption–adsorption isotherm was of type I isotherm typical of microporous solids having relatively small external surfaces as defined by the International Union of Pure and Applied Chemistry (IUPAC) classification (Thommes et al., 2015).

3.1.2. Effect of pH vs coagulant dosage

The WW was observed to have a high content of turbidity and TSS (Table 1), therefore, a CFD process was applied to reduce these parameters. Considering the lack of information regarding the efficiency of the NOCs developed for the treatment of WW, in this step the pH and coagulant dosage were varied and DOC, turbidity and TSS removal was accessed (Figure S.1). The results showed that NOCs and ferric chloride were influenced by both pH and coagulant dosage. Although, at pH 3.0 it is observed higher DOC removals with the application of NOCs, an evaluation of the turbidity and TSS removal showed that all coagulants achieved their highest efficiency at pH 3.0 as well. However, the dosage required for each coagulant was observed to be different (2.0, 2.0, 0.1, 0.1, 0.1 and 0.5 g/L, respectively, for DG seeds, FA seeds, DC seeds, TV seeds, rachis and ferric chloride).

The actions of NOCs in treatment of the WW lies in the presence of water-soluble dimeric proteins present in the seeds and rachis, as previously detected by the FTIR analysis. These proteins work as natural polyelectrolytes, with a mechanism that combines adsorption (due to the porous structure observed in the SEM images), charge neutralization, particle bridging of destabilized particles, enmeshment and precipitation (Beltrán-Heredia et al., 2012; Camacho et al., 2017; Vunain et al., 2019). Due to these mechanisms, when NOCs are applied to the WW, the protein in the seeds binds to the negatively charged particles that cause turbidity, such as clays, bacteria, dust, among others, to form heavier flocs which precipitate.

When ferric chloride is added to the WW at pH 3.0, a number of parallel and sequential reactions occur. Initially, the ferric chloride is dissociated to yield the trivalent Fe^{3+} ions (Equation (10)). The trivalent ion Fe^{3+} then hydrate to form the aquometal complex $Fe(H_2O)_6^{3+}$. This aquometal then lose protons to form a series of soluble mononuclear species, such as $Fe(HO)^{2+}$ and $Fe(HO)_2^{+}$ (Howe et al., 2012).

$$FeCl_3 \leftrightarrow Fe^{3+} + 3Cl^- \qquad \text{Equation 10}$$

These species promote positive or negative charges, depending on

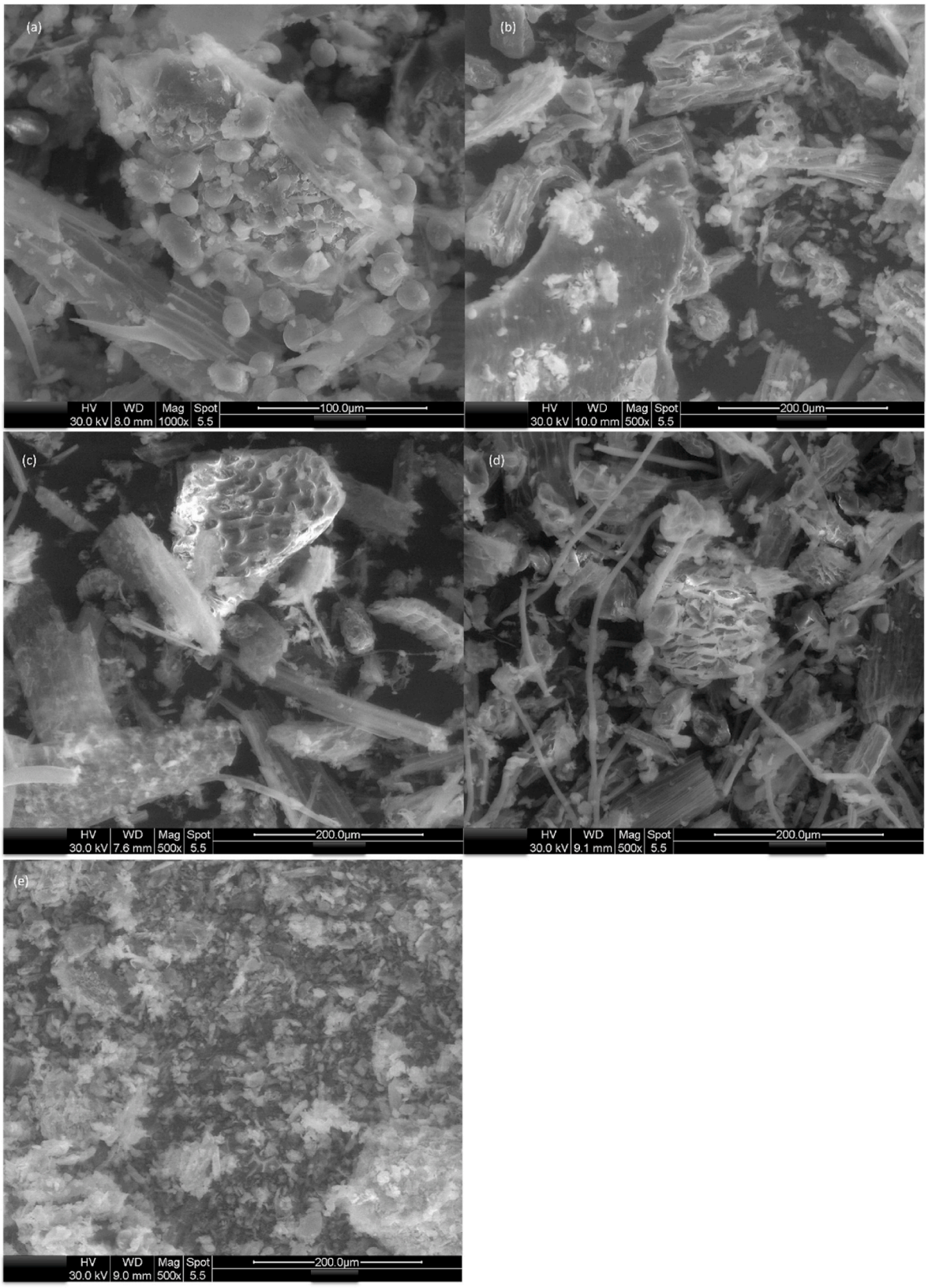

Fig. 2. Scanning electron microscopy of (a) DG seeds, (b) DC seeds, (c) FA seeds, (d) TV seeds and (e) rachis.

the pH. Generally, these species are positively charged at a pH lower than 6.0. These positively charged hydrolysis species can absorb on the colloidal particles surface, originating their destabilization. This mechanism in known as charge neutralization, and the agglomeration into heavier particles, leads to precipitation (Amaral-Silva et al., 2016).

3.1.3. *Optimization of mixing parameters on coagulation process*

To achieve a good flocculation, the mixing time must be considered

Table 4
NOC characterization of iron, copper, sodium, potassium, calcium and magnesium.

Coagulants	Iron	Copper	Sodium	Potassium	Calcium	Magnesium
	mg/L	mg/L	mg/L	mg/L	mg/L	mg/L
DG seeds	6.3	0.2	624.2	184.1	104.2	110.2
DC seeds	1.8	1.2	670.6	986.6	751.5	190.1
FA seeds	4.2	0.4	633.1	126.4	155.7	102.1
TV seeds	2.2	0.4	626.4	633.1	311.6	126.1
Rachis	2.0	1.2	647.3	1237	322.8	137.4

Table 5
Specific surface areas and pore characteristics of NOCs.

Coagulants	S_{BET} (m^2/g)
DG seeds	0.04
DC seeds	0.04
FA seeds	0.16
TV seeds	0.00
Rachis	0.45

as a differentiating factor. To perform the CFD process, two steps are performed, a fast mix which ensures a dispersion of the coagulant in the WW and a slow mix, which ensures the generation and aggregation of small flocs in the water. To understand how the mixing conditions affects the efficiency of the coagulants, the fast mix and slow mix were varied, with application of the conditions set in Table 3. The results showed that coagulants DG seeds and FA seeds required faster agitation speed (mix 5) to achieve higher removals. On the other hand, DC seeds, TV seeds, rachis and ferric chloride achieved the best removals wit application of lower agitation speed (mix3, mix 2, mix 2 and mix 1, respectively). Under these conditions, DOC removal achieved 15.5, 14.1, 15.0, 26.2, 44.9 and 27.5% removal respectively, turbidity removal achieved 98.9, 97.2, 86.2, 92.0, 93.0 and 90.3% respectively and TSS removal achieved 94.9, 93.2, 85.0, 89.0, 90.8 and 87.7% respectively, for DG seeds, FA seeds, DC seeds, TV seeds, rachis and ferric chloride (Fig. 3).

The application of higher agitation speed affected the performance of the coagulants, because, as the particle size increases, the faster mixing speed agitation broke up the existing flocs as a result of disruptive forces and the collision efficiency of the particles in a shear field decreased (Domínguez et al., 2007). It is also necessary to consider the dynamic

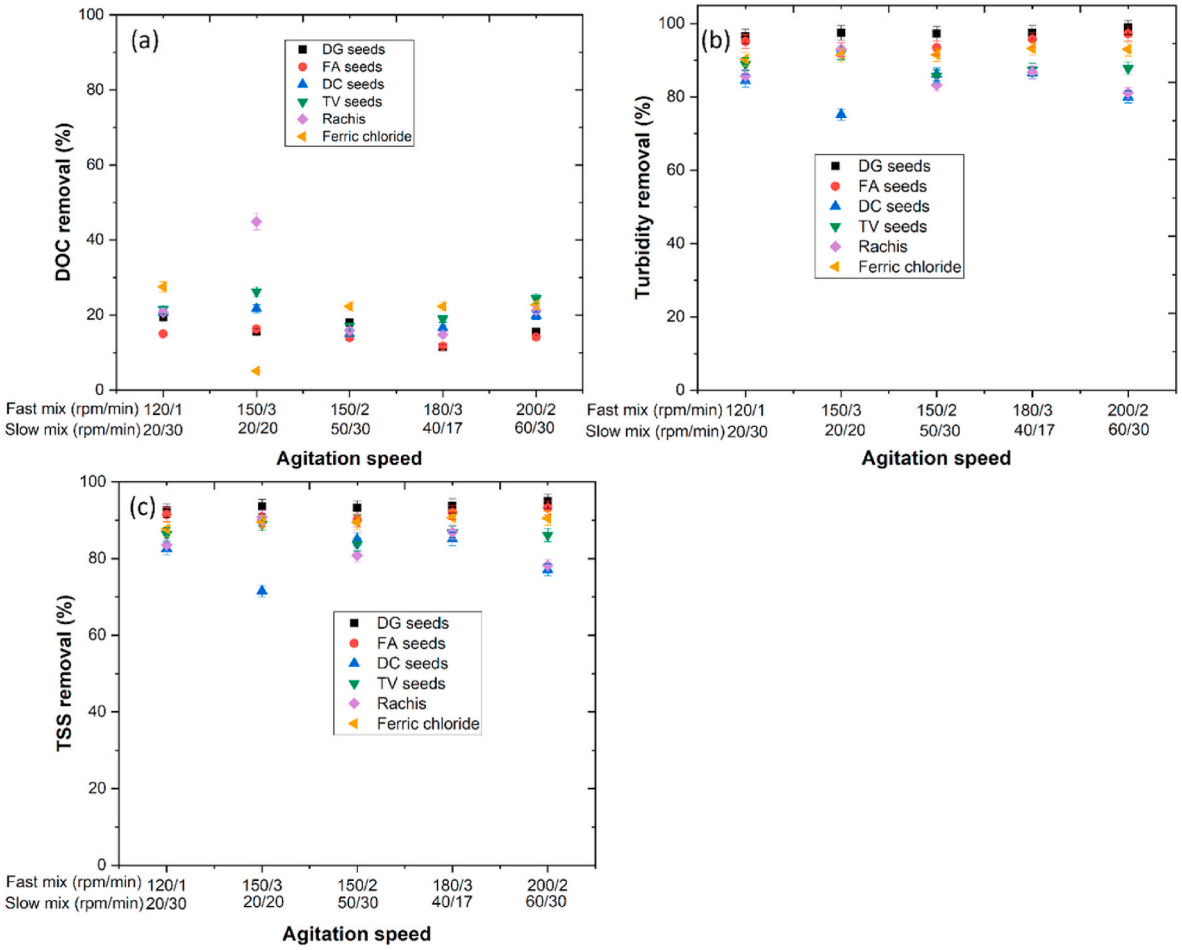

Fig. 3. Evolution of (a) DOC, (b) turbidity and (c) TSS removal throughout the *CFD* experiments, using different mixing conditions ($[DOC]_0$ = 400 mg C/L, turbidity = 296 NTU, TSS = 750 mg/L, 2.0, 2.0, 0.1, 0.1, 0.1 and 0.5 g/L for DG seeds, FA seeds, DC seeds, TV seeds, rachis and ferric chloride, pH = 3.0, temperature 298 K, sedimentation time 12 h).

balance between floc growth and breakage which often leads to a steady-state floc-size distribution, where the limiting size depends on the applied shear rate. If the shear rate applied is increased to a certain point, the pre-formed flocs can be broken. In the case of sweep-floc coagulation, this breakage in not fully reversible, and flocs do not completely re-form when the original shear conditions are restored, which explains the decrease in efficiency, when agitation speed is increased.

3.2. Treatment of winery wastewater with application of AOPs

3.2.1. Effect of AOP variation

In the previous sections, it was observed that CFD process could only remove organic carbon to some extent. Therefore, a more suitable treatment process is required to decrease the DOC present in the WW. In this section, different AOPs ((1) H_2O_2, (2) UV-C, (3) UV-C + H_2O_2, (4) UV-C + Fe^{2+}, (5) H_2O_2 + Fe^{2+} (Fenton process), (6) H_2O_2 + UV-C + Fe^{2+} (photo-Fenton process)) were tested, to evaluate which is the most efficient in the degradation of DOC. In Fig. 4(a) it is shown the DOC removal in function of time and in Fig. 4(b) is shown the H_2O_2 consumptions.

The results showed that application of H_2O_2, UV-C + Fe2+ and UV-C had little oxidation power, revealing low organic carbon degradation (12.3, 13.7 and 15.6%, respectively). The combined action of H_2O_2 + UV-C achieved higher DOC removal with 32.9% in 240 min. The Fenton process, which involved the application of H_2O_2 + Fe^{2+} achieved a DOC removal OF 22.9% after 240 min. The application of photo-Fenton process achieved the highest DOC removal, with 84.9%.

Considering these results, the relative efficiencies of the processes tested above are in the following order: H_2O_2 + UV-C + Fe^{2+} (photo-Fenton) > H_2O_2 + UV-C > H_2O_2 + Fe^{2+} (photo-Fenton) > UV-C > UV-C + Fe^{2+} > H_2O_2. The highest efficiency observed with the photo-Fenton process is due to the production of more hydroxyl radicals ($HO^{\bullet}$) than Fenton process and other processes, due to the higher consumption of H_2O_2, as observed in Fig. 4(b). These results indicate that the UV-C lamp has a synergistic effect when combined with the Fenton process enhancement in the degradation of the organic matter.

With the combination of UV and H_2O_2 the chemical bonds of the organic compounds present on the WW can be directly photolyzed by UV radiation and rapidly improved in the presence of H_2O_2 (Ince et al., 1997; Teixeira et al., 2022). Adding Fe^{2+} to UV-C and UV-C light can remove DOC, but to a smaller percentage. At last, the H_2O_2 alone has the lowest influence on DOC removal, thus the results allow the conclusion that the oxidizing power of H_2O_2 is not enough to bring about the degradation of organic carbon.

In all the experiments, the DOC degradation can be described as a pseudo first-order kinetic, in which $\ln[DOC] = -kt + \ln[DOC]_0$ and a plot is charted applying $\ln[DOC/DOC_0]$ as a function of time (t). regarding TOC concentration as it is observed from the data in Table 6. Also, to have a better knowledge on the removal of organic carbon, it is presented the time necessary to reduce to 50% the initial concentration of total organic carbon from the WW – the half-life time ($t_{1/2} = 0.693/k$).

As it can be seen in Fig. 4 and comparing k values and $t_{1/2}$ in Table 6, photo-Fenton process is the most efficient process on DOC removal regarding other processes. This fact is due to the synergistic effect of UV-C radiation. The low-pressure mercury vapor lamp TNN 15/32 has little power, only 15 W, however the use of a simple UV lamp in Fenton reaction is very important to increase the efficiency of DOC degradation. This is because the UV light wavelength can significantly influence direct formation of $HO^{\bullet}$ radicals by photolysis of the H_2O_2 (as observed in Fig. 4(b)) as well as the photo-reduction of Fe^{3+} to Fe^{2+}, increasing the reaction's kinetic rate. In order to have a complete knowledge of the optimal conditions for the process of photo-Fenton process, the next steps of this work are to assess the capacity of photo-Fenton process to oxidize organic carbon, evaluating each parameter fixing the values of the others.

3.2.2. Optimization of pH on photo-Fenton oxidation

In this section, the pH was varied (3.0–11.0) under the following operational conditions: $[DOC]_0 = 400$ mg/L, $[Fe^{2+}] = 2.5$ mM, agitation 350 rpm, reaction time 240 min, radiation UV-C lamp (254 nm), temperature 298 K. Fig. 5(a) shows that the pH significantly influences the mineralization of organic carbon by photo-Fenton process, with the highest removal obtained at pH 3.0 (84.9%). With application of pH 5.0, 7.0, 9.0 and 11.0, the DOC removal results showed a significant decrease

Table 6
Pseudo first-order rate kinetics (k) and half-life ($t_{1/2}$) of DOC removal from WW. Means in the same column with different letters represent significant differences ($p < 0.05$) within each parameter (k and $t_{1/2}$) by comparing AOPs.

Oxidation process	kx10^{-3} ± SDx10^{-3} (min^{-1})	$t_{1/2}$ (min)
H_2O_2	0.317 ± 0.016 a	2186.1 ± 43.7 a
UV	0.402 ± 0.020 b	1723.9 ± 34.5 b
UV + Fe^{2+}	0.333 ± 0.017 b	2081.1 ± 41.6 c
UV + H_2O_2	1.50 ± 0.075 c	462.0 ± 9.2 d
Fenton	0.854 ± 0.043 d	811.5 ± 16.2 e
Photo-Fenton	6.89 ± 0.040 e	100.6 ± 2.0 f

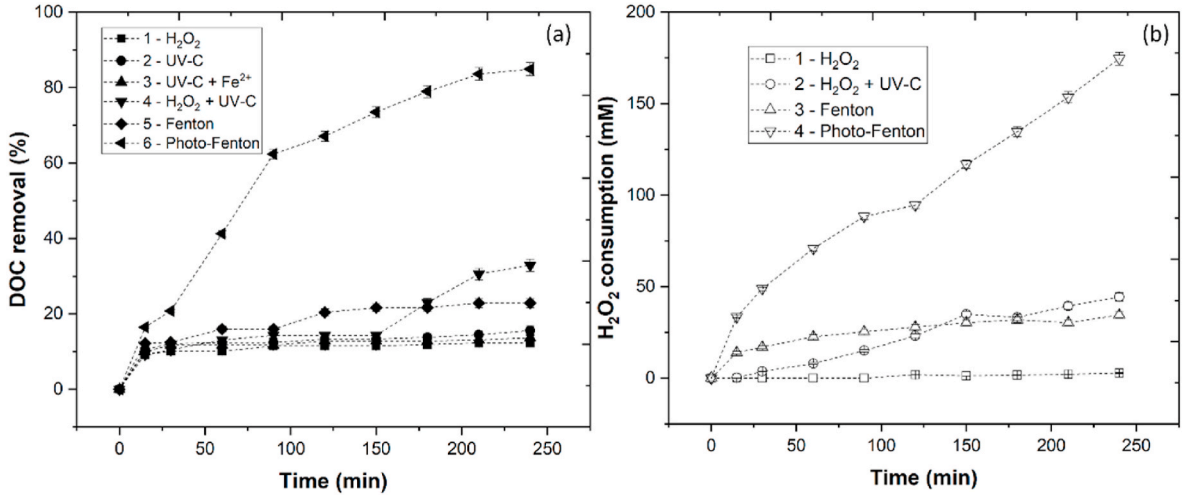

Fig. 4. (a) DOC removal, (b) H_2O_2 consumption with application of different AOPs, under different conditions ($[DOC]_0 = 400$ mg C/L, $[Fe^{2+}] = 2.5$ mM, pH = 3.0, temperature 298 K, UV-C lamp = TNN 15/32 *Heraeus*).

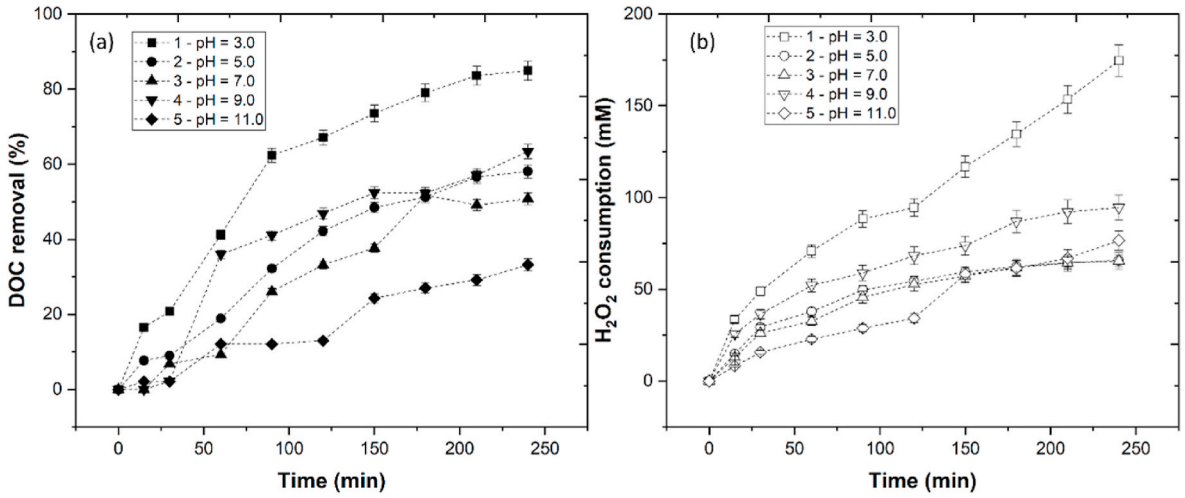

Fig. 5. (a) DOC removal, (b) H_2O_2 consumption with variation of WW pH (3.0–11.0) in photo-Fenton process ($[DOC]_0 = 400$ mg C/L, $[Fe^{2+}] = 2.5$ mM, radiation UV-C mercury lamp (254 nm), agitation 350 rpm, temperature 298 K, reaction time 240 min).

to 58.1, 50.8, 63.4 and 33.2%, respectively, for pH 5.0, 7.0, 9.0 and 11.0.

In these reactions three factors influences the oxidation process of photo-Fenton: (1) the iron, (2) the hydrogen peroxide and (3) the pH. The decrease of activity for pH values below the optimum is understandable considering that Fe^{3+} forms different species in solution, and the quantum yield of light absorption by Fe^{3+} is directly depending on the specific species responsible for the absorption. The main specie observed at pH 3.0, $Fe(OH)^{2+}(H_2O)_5$ is one with the largest light absorption coefficient and quantum yield for $HO^{\bullet}$ radical production, along with Fe^{2+} regeneration in the range of 280–370 nm (Perez et al., 2002), which explains the high DOC removal at pH 3.0. For higher pH solutions(alkaline), the presence of $Fe(OH)_2^+(H_2O)_4$ dominates, but the solution becomes unstable with $Fe(OH)_3$ precipitation (Benkelberg and Warneck, 1995; Perez et al., 2002), which blocks the decomposition of hydrogen peroxide catalyzed by the ferrous iron (Lucas and Peres, 2007). In Fig. 5(b), it is observed that by increasing the pH > 3.0, the H_2O_2 consumption decreases significantly, thus decreasing the DOC degradation efficiency of the photo-Fenton process. These results are in agreement with the work of Çalık and Çifçi (2022), who observed that Fenton process achieved the highest efficiency in the treatment of a textile industry wastewater at pH 3.0. However, unlike this work, the consumption of H_2O_2 was much lower (8.82 mM), than the concentration consumed in this work. The difference between the treatment of textile dyes and WW was previously reported by Rodríguez-Chueca et al. (2017), who observed that the degradation of organic matter from WW required more demanding treatments with higher dosages of reagent regarding the treatment of dyes.

3.2.3. *Optimization of Fe^{2+} concentration on photo-Fenton oxidation*

In this section, the effect of Fe^{2+} concentration on the mineralization of organic carbon of red WW was studied. The Fe^{2+} concentration was varied within the range of 0.5–5 mM (Fig. 6(a)) and results showed a DOC removal of 81.6, 84.1, 84.9 and 82.5%, respectively, for 0.5, 1.0, 2.5 and 5.0 mM Fe^{2+}.

The results indicated that the extent of DOC degradation increased with the increase in initial Fe^{2+} concentration, from 0.5 to 2.5 mM. However, the increase from 2.5 to 5.0 mM Fe^{2+} decreased the DOC removal. These results can be explained by the redox reactions since $HO^{\bullet}$ and $HO_2^{\bullet}$ radicals may be scavenged by the excess of Fe^{2+} as observed by Equation 11 – Equation (13) (Lucas and Peres, 2009).

$$Fe^{2+} + HO^{\bullet} \rightarrow Fe^{3+} + HO^{-} \quad \text{Equation 11}$$

$$Fe^{2+} + HO_2^{\bullet} \rightarrow Fe^{3+} + HO_2^{-} \quad \text{Equation 12}$$

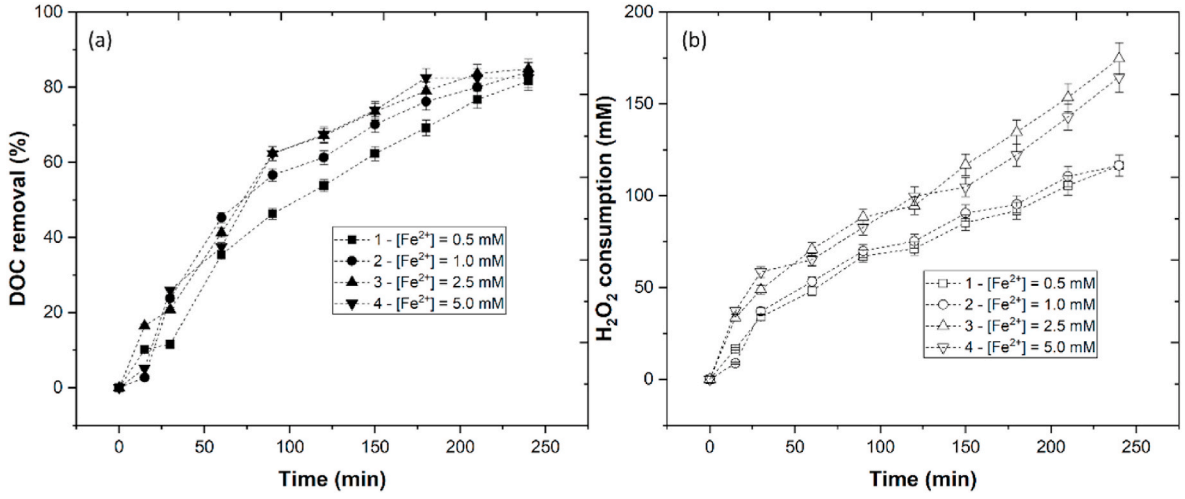

Fig. 6. (a) DOC removal, (b) H_2O_2 consumption with application of different Fe^{2+} concentrations (0.5–5.0 mM) in photo-Fenton process ($[DOC]_0 = 400$ mg C/L, pH = 3.0, radiation UV-C mercury lamp (254 nm), agitation 350 rpm, temperature 298 K, reaction time 240 min).

$$Fe^{3+} + HO_2^{\bullet} \rightarrow Fe^{2+} + O_2(2) + H(+) \quad \text{Equation 13}$$

The addition of 2.5 and 5.0 mM Fe^{2+} also had the highest consumption of H_2O_2, regarding 0.5 and 1.0 mM Fe^{2+} (Fig. 6(b)), meaning that DOC removal was directly linked to the consumption of hydrogen peroxide, and at the same time to the production of $HO^{\bullet}$ radicals.

3.2.4. Effect of KPS and PMS addition to photo-Fenton process

In order to increase the rate of DOC degradation, different concentrations of KPS and PMS (0.5, 1.0, 2.5 and 10 mM) were applied in combination with the optimal experimental conditions obtained in Section 3.2.3. The results shown in Fig. 7(a) and Fig. 7(c), revealed a DOC degradation of 91.2 and 88.0%, respectively, for 1.0 mM of KPS and PMS. As previously observed, the sulfate radicals can be activated either by UV radiation or application of a catalyst, and when applied, the reactions described by Equation (14) to Equation (20) takes place in DOC degradation (Khataee et al., 2016), leading to the production of sulfate radicals.

$$2HO^{\bullet} \rightarrow H_2O_2 \quad \text{Equation 14}$$

$$S_2O_8^{2-} + h\nu \rightarrow 2SO_4^{\bullet-} \quad \text{Equation 15}$$

$$SO_4^{\bullet-} + HO^{\bullet} \rightarrow 2SO_4^{\bullet-}H^+ + SO_4^{2-} + 0.5O_2 \quad \text{Equation16}$$

$$2SO_4^{\bullet-} \rightarrow S_2O_8^{2-} \quad \text{Equation17}$$

$$SO_4^{\bullet-} + S_2O_8^{2-} \rightarrow SO_4^{2-} + S_2O_8^{\bullet-} \quad \text{Equation18}$$

$$SO_4^{\bullet-} + H_2O \rightarrow SO_4^{2-} + HO^{\bullet} + H^+ \quad \text{Equation19}$$

$$Fe^{2+} + S_2O_8^{2-} \rightarrow Fe^{3+} + SO_4^{\bullet-} + SO_4^{2-} \quad \text{Equation 20}$$

The results showed that KPS was more reactive than PMS, due to the fact that the photolysis of PMS produces 1 mol of sulfate radical and 1 mol of hydroxyl radical per each mole of peroxymonosulphate (Rodríguez-Chueca et al., 2017), and the photolysis of KPS produces 2 mol of sulfate radical (Boczkaj and Fernandes, 2017). Also the efficiency of KPS is explained based on the reactivity of the persulfate anion ($S_2O_8^{2-}$; E° = 2.01 V), comparatively to PMS, in which the peroxymonosulfate anion presents lower reactivity (HSO_5^-; E° = 1.85 V) (Boczkaj and Fernandes, 2017).

The addition of 10 mM KPS and PMS had the lowest degradation of DOC (74.1 and 71.0% respectively). These results can be explained by the competition between the organic matter present in the WW and the excess of persulfate in solution for the $SO_4^{\bullet-}$ and $HO^{\bullet}$ radicals (Equation (21) to Equation (24)). Similar results were obtained in the works of Khataee et al. (2016) and Xu et al. (2019), in the treatment of textile dye acid red 73 and contaminant 2,4-dinitrotoluene, by the combined application of persulfate and H_2O_2.

$$S_2O_8^{2-} + H_2O_2 \rightarrow 2SO_4^{2-} + 2H^+ + O_2 \quad \text{Equation21}$$

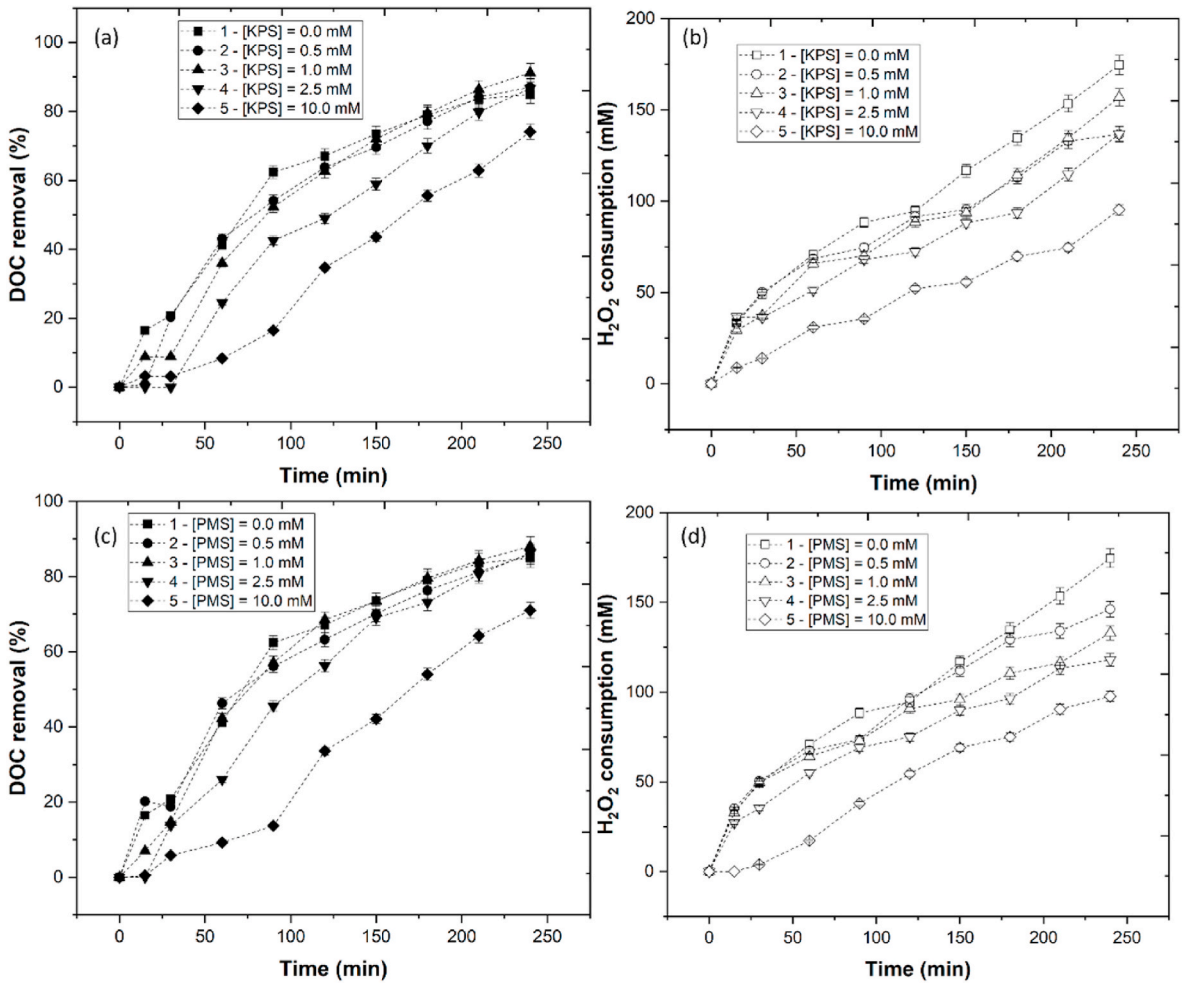

Fig. 7. Effect of KPS addition to photo-Fenton process in (a) DOC removal, (b) H_2O_2 consumption. Effect of PMS addition to photo-Fenton process in (c) DOC removal, (d) H_2O_2 consumption. ($[DOC]_0$ = 400 mg C/L, $[Fe^{2+}]$ = 2.5 mM, pH = 3.0, radiation UV-C mercury lamp (254 nm), agitation 350 rpm, temperature 298 K, reaction time 240 min).

$$S_2O_8^{2-} + HO^{\bullet} \rightarrow S_2O_8^{\bullet-} + HO^{-} \quad \text{Equation 22}$$

$$SO_4^{\bullet-} + S_2O_8^{2-} \rightarrow S_2O_8^{\bullet-} + S_2O_4^{2-} \quad \text{Equation23}$$

$$SO_4^{\bullet-} + SO_4^{\bullet-} \rightarrow S_2O_8^{2-} \quad \text{Equation24}$$

One of this work's objective is the study of the separation of wastewaters from the production of red and white WW, to understand how the chemical composition of the WW influences the efficiency of the AOPs. In this section, the photo-Fenton, KPS-photo-Fenton and PMS-photo-Fenton were applied in the treatment of a white WW with the same DOC concentration (400 mg C/L) as the red WW. The results presented in Fig. 8(a), shows that application of photo-Fenton reached a DOC removal of 86.5% after 240 min of reaction. When KPS and PMS were added to the photo-Fenton process, DOC removal increased to 96.8 and 91.5%, respectively. The effect of KPS and PMS was similar to the treatment of red WW, however, the results obtained with addition of KPS revealed higher. Therefore, these results suggest that the white WW is more sensitive to degradation by KPS-photo-Fenton. These results support the initial objective, of separating the red and white WW, to facilitate the DOC degradation.

3.3. Application of combined CFD-AOPs

In the previous sections it was observed that the CFD process had a good capacity to decrease the solid particles in suspension in the WW, however, low DOC removal was observed with the application of this process. With application of AOPs, DOC removal achieved higher results, however, several disadvantages were associated to this process, such as long reaction times and high H_2O_2 consumption. In this section, the CFD process was applied to the red and white WW as a pre-treatment. This pre-treatment allowed a high removal of turbidity and TSS which were responsible for the WW dark color. In addition to turbidity and TSS, total polyphenols (TPh) removal were also evaluated, with results showing a 77.8, 84.5, 80.9, 89.7, 80.9 and <0.5%, respectively, for application of DG seeds, FA seeds, DC seeds, TV seeds, rachis and ferric chloride in red WW. With application of NOCs to white WW, it was observed a 55.4, 76.1, 88.0, 92.2, >99.5 and <0.5%, respectively (Fig. 9). With exception to ferric chloride, NOCs revealed to be very efficient in the removal of TPh from WW. Considering that these NOCs were never applied before in the treatment of WW, the effects in TPh removal were still unknown, however, these results were similar to other plant-based coagulants such as derived from *Moringa oleifera* (MO). In the work of Rifi et al. (2022), a coagulant derived from MO showed a 96 and 86% removal efficiency of turbidity and TPh from a olive mill wastewater. The removal of TPh content is important because they are responsible for the WW color and represent a toxicity to the environment, due to the difficulty of microorganisms to degrade cycling compounds (Jorge et al., 2021, 2022a).

The removal of turbidity, TSS and TPh from the WW by the NOCs influenced the DOC removal. The results in Fig. 10(a), showed that the application of NOCs in combination with KPS-photo-Fenton for the treatment of red WW achieved a DOC removal of 96.0, 95.9, 94.6, 94.6 and 96.3%, respectively, for DG seeds, FA seeds, DC seeds, TV seeds and rachis. When this treatment was applied to white WW (Fig. 10(b)), it was observed a DOC removal of 97.4, 97.9, 97.4, 97.7 and 98.2%, respectively. NOCs improved DOC removal, clearly driven by the removal of turbidity, TSS and TPh from the WW, which from one hand blocked the radiation, reducing the rate of regeneration of Fe^{3+} into Fe^{2+} and on another hand, the particles in suspension competed for the $HO^{\bullet}$ radicals. These results are in agreement with the work of Amor et al. (2015), who observed that the excess of sediments in the landfill leachate reduced the efficiency of photo-Fenton process and that combining CFD process with photo-Fenton increased the DOC removal.

When ferric chloride was applied, the opposite effect was observed, as DOC removal achieved 89.8 and 93.7%, respectively, for red and white WW, which are lower than the values obtained by application of KPS-photo-Fenton without CFD pre-treatment. These results can be explained by the presence of the excess of ferric iron present in the WW after treatment with ferric chloride (106.0 and 103.3 mg Fe/L respectively, for red and white WW), which acted as scavenger of $SO_4^{\bullet-}$ and $HO^{\bullet}$ (Lucas and Peres, 2009; Wang and Chu, 2012) radicals as observed on Equation (11) and Equation (25), which in turn decreased the KPS-photo-Fenton process efficiency on carbon degradation.

$$Fe^{2+} + SO_4^{\bullet-} \rightarrow Fe^{3+} + S_2O_4^{2-} \quad \text{Equation25}$$

Although the results showed high DOC removal with the application of combined CFD-photo-Fenton process, this parameter indicates only the dissolved carbon in the WW. Therefore, a more conclusive analysis is required, such as COD and BOD_5, which indicates the carbon that is dissolved and undissolved. The application of NOCs in the treatment of red WW showed a COD removal of 24.9, 29.5, 29.5, 33.4, 25.6 and 49.7%, respectively (Fig. 11(a)). When NOCs were applied for the treatment of white WW, results showed a COD removal of 26.6, 23.1, 33.7, 24.8, 52.4 and 35.5%, respectively (Fig. 11(b)). The BOD_5 was also investigated, with results showing a removal of 1.8, 1.8, 0.5, 12.7, 5.5

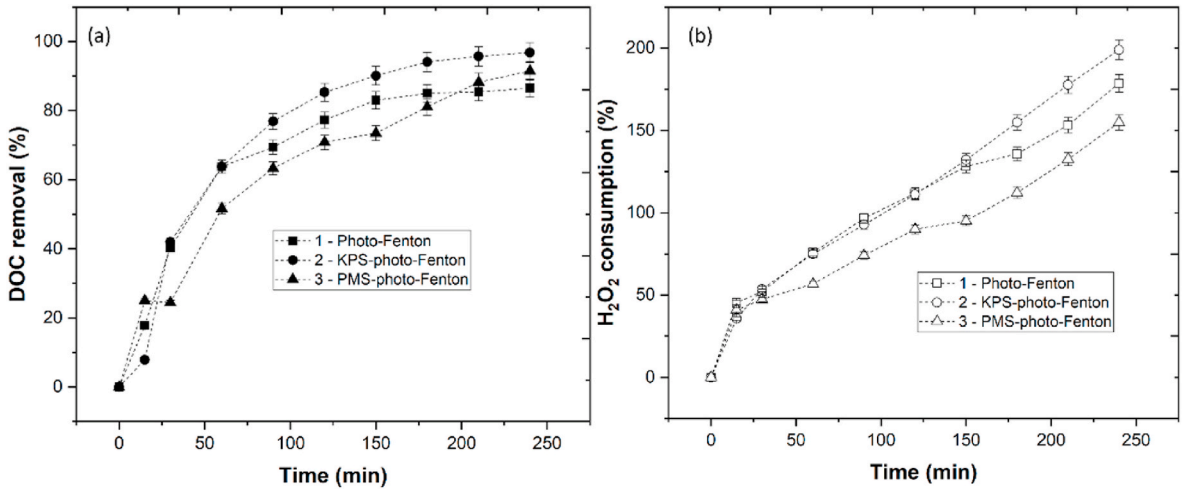

Fig. 8. Effect of photo-Fenton, KPS-photo-Fenton and PMS-photo-Fenton in (a) DOC removal, (b) H_2O_2 consumption in the treatment of white WW ($[DOC]_0$ = 400 mg C/L, $[Fe^{2+}]$ = 2.5 mM, [KPS] = 1.0 mM, [PMS] = 1.0 mM, pH = 3.0, radiation UV-C mercury lamp (254 nm), agitation 350 rpm, temperature 298 K, reaction time 240 min).

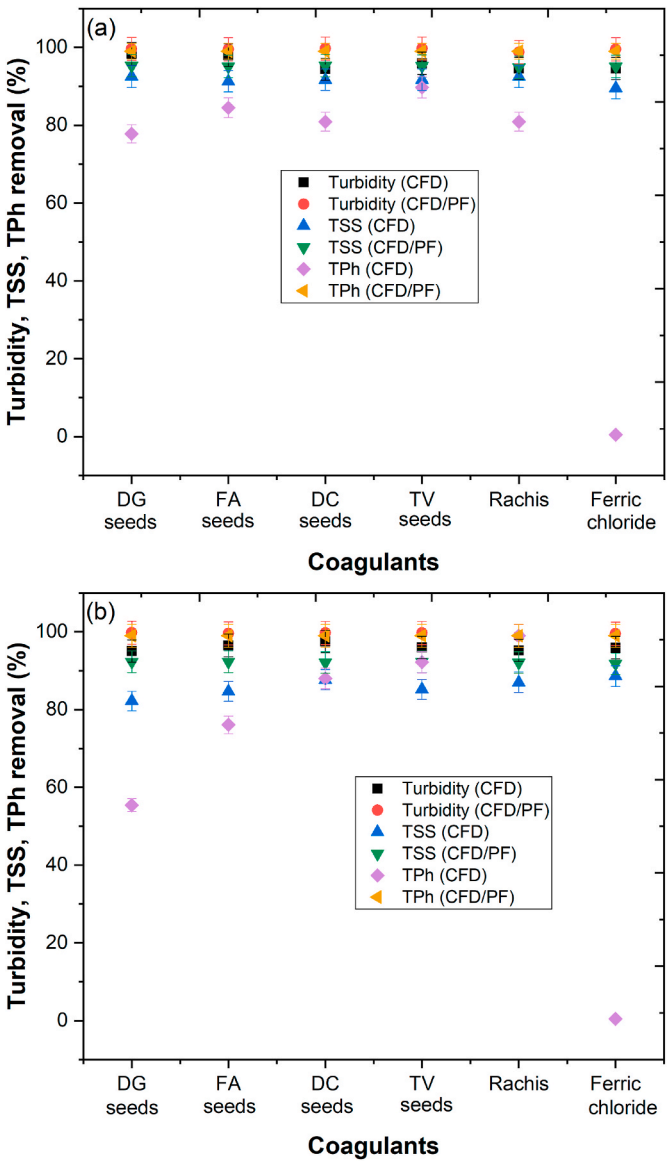

Fig. 9. Influence of CFD and CFD/PF in the removal of turbidity, TSS and TPh from (a) red WW and (b) white WW. CFD – coagulation-flocculation-decantation, PF – photo-Fenton. (For interpretation of the references to color in this figure legend, the reader is referred to the Web version of this article.)

and 75.0%, respectively, for red WW and 20.0, 32.5, 22.9, 22.9, 83.9 and 33.6%, respectively for white WW. These results can be related with the removal of turbidity, TSS and TPh, in which their removal led to the removal of the undissolved carbon. With the application of KPS-photo-Fenton, the COD and BOD_5 removal reached the legislated value for wastewater discharge (150 and 40 mg O_2/L, respectively) in accordance with the Portuguese Decree Law n° 236/98.

The biodegradability (BOD_5/COD) of the WW was evaluated, considering that both red and white WW presented low biodegradability (0.26 and 0.37). The application of NOCs was observed to have increased the biodegradability of red and white WW. With application of KPS-photo-Fenton, the biodegradability increased further in red WW pre-treated with DC seeds and rachis (0.61 and 0.98, respectively) and in white WW pre-treated with FA and DC seeds (0.58 and 0.75, respectively). These results were in agreement with the work of Barros et al. (2020), who observed that the combination of CFD process with Fenton process increased the biodegradability of the coffee processing wastewater (CPW) from 0.34 to 0.47. The results obtained in this work also showed that the matrix of the wastewater is important, considering that ferric chloride decreased the biodegradability of red WW (0.26) and increased the biodegradability of white WW (0.38). Although the combined CFD-KPS-photo-Fenton processes could improve wastewater biodegradability, it was not advisable to introduce the WW into a biologic process, because the COD concentration remaining was very low. Ideally, the photo-Fenton process should be used until legal discharge limits are achieved.

3.4. Energy consumption and operational cost

The combination of CFD with KPS-photo-Fenton proved to be very efficient in terms of organic matter degradation, however, these data are nor enough to answer the question of whether these processes are economical in terms of energy consumption and operational cost. To evaluate the energy consumption of the system, the electric energy per g of DOC (E_{EM}) was determined (Equation (26)).

$$E_{EM} = \frac{Pxt}{(DOC_i - DOC_f)xV} x1000 \qquad \text{Equation 26}$$

This parameter is defined as the electric energy in kilowatts hours (kWh) required to degrade 1 g of DOC in wastewater, where P is the power of the UV-C lamp (kW), t is the time (h), V is the volume (dm^3) of the treated wastewater and DOC_i and DOC_f are the initial and final concentrations of DOC, respectively (Dükkancı, 2018). To access the cost of the treatment, the E_{EM} was multiplied by medium value of electricity cost in Portugal (0.080 €/kWh). The reagent cost was also access, with reagents costs assumed as: 0.25 € L^{-1} for H_2O_2 solution 30% (w/v), 0.082 € kg^{-1} for $FeSO_4 \bullet 7H_2O$ and 0.018 € kg^{-1} for KPS (Lucas et al., 2010). The application of the combined CFD + KPS-photo-Fenton process increased the E_{EM} values regarding the application of KPS-photo-Fenton process in both red and white WW treatment (Table 7), which undoubtably increased the cost associated to the energy consumption. This fact is related to the degradation of lower concentrations of DOC, due to the previous removal by CFD, in a similar time. However, when the total cost is analyzed, the results show a significant decrease of the total costs with application of the combined process. The only exception was the application of ferric chloride as a coagulant, which increased significantly the cost of treatment. One explanation is the reduction of the H_2O_2 used for the reaction within the application of the combined process, which decreased the costs. When ferric chloride was applied, the excess of iron acted as a scavenger for $HO^{\bullet}$, decreasing the efficiency of the reaction, and at the same time increasing the costs of the WW treatment. These results are in agreement with the work of Lak et al. (2018), who observed that the application of the CFD process as a pre-treatment decreased the energy consumption of the oxidation process, in the treatment of landfill leachate.

Based in the results obtained in this work, it could be possible throughout the control of a certain number of variables in CFD (pH, coagulant concentration, mixing conditions, sedimentation time) and AOPs (pH, oxidant and catalyst concentrations and radiation source), to apply these treatments in an upgraded scale, with a reduced operational cost. However, certain challenges need to be in concern when upscaling the treatment from batch to pilot, such as (1) treatment in plants operated in a continuous mode, (2) higher concentrations of coagulant are required in full-scale wastewater treatment and (3) controlling the ratio of oxidants used in AOP treatments, which could lead to higher treatment costs. However, the availability and the low cost related with the plant sub-products will reduce the treatment cost of the oxidation processes, overcoming the usually significant costs of agro-industrial wastewaters treatments.

4. Conclusions

This work addresses the treatment of a WW by application of a

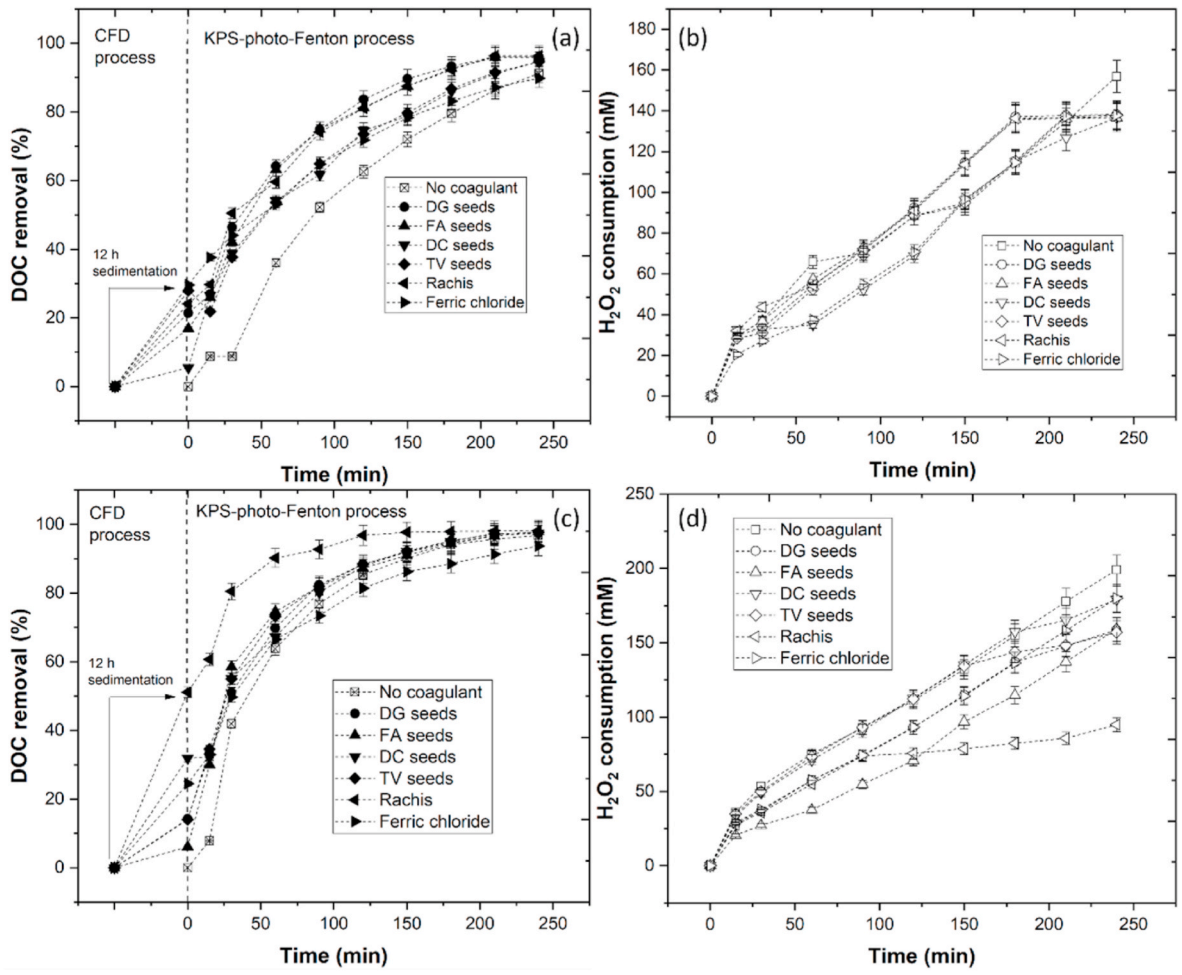

Fig. 10. Influence of CFD and KPS-photo-Fenton process in DOC removal of (a) red WW, (c) white WW and H_2O_2 consumption of (b) red WW, (d) white WW.

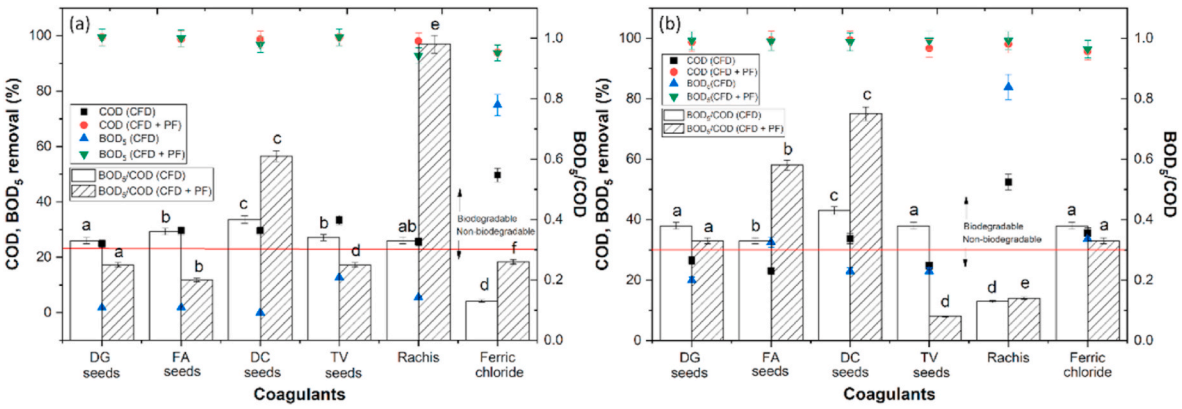

Fig. 11. Effect of CFD and CFD + photo-Fenton (PF) processes in the CFD and BOD_5 removal and biodegradability of (a) red WW and (b) white WW. Means in bars with different letters represent significant differences ($p < 0.05$) within biodegradability (BOD_5/COD) by comparing treatment processes. (For interpretation of the references to color in this figure legend, the reader is referred to the Web version of this article.)

physical-chemical process (CFD) followed by a chemical process (AOP). To perform CFD process, 5 different NOCs were developed and by FTIR analysis it is concluded that these materials are organic in nature, with proteins, fatty acids, carbohydrates and lignin in their constitution. In addition, SEM analysis shows that NOCs are porous materials, with adsorption capacity. Based in the results, it is concluded that NOCs are dependent on the pH of the WW, the dosage applied and mixing conditions, reaching a turbidity removal between 86.2 and 98.9%, a TSS removal between 85.0 and 94.9% and a TPh removal between 77.8 and 89.7%. Different AOPs were applied and with the results obtained, it is concluded that photo-Fenton process is the most efficient process. The photo-Fenton process was optimized, with application of KPS, with results showing an increase of DOC removal from 84.9 to 91.2%, respectively. In this work it was also explored the treatment of a red and white WW separately, with results showing a DOC removal of 91.2 and 96.8%, respectively, with application of KPS-photo-Fenton, thus it is concluded

Table 7
Electric energy per mass (E_{EM}), energy cost, reagent cost and total cost after treatment of red and white WW. Means in the same column with different letters represent significant differences ($p < 0.05$) within each parameter (E_{EM}, energy cost, reagent cost and total cost) by comparing treatment processes.

Process	E_{EM}	Energy cost	Reagent cost	Total cost
	kWh/g DOC	€/g/L DOC	€/g/L DOC	€/g/L DOC
Red WW				
AOP	0.328 ± 0.02 a	0.026 ± 0.001 a	2.02 ± 0.02 a	2.05 ± 0.01 a
DG + AOP	0.401 ± 0.02 bd	0.032 ± 0.001 b	1.78 ± 0.02 b	1.81 ± 0.01 b
FA + AOP	0.380 ± 0.01 bd	0.030 ± 0.001 b	1.76 ± 0.02 c	1.79 ± 0.01 bc
DC + AOP	0.336 ± 0.02 a	0.027 ± 0.001 a	1.76 ± 0.02 bc	1.79 ± 0.01 c
TV + AOP	0.449 ± 0.03 cd	0.036 ± 0.002 c	1.78 ± 0.01 bc	1.81 ± 0.01 b
Rachis + AOP	0.415 ± 0.02 d	0.033 ± 0.001 b	1.77 ± 0.01 bc	1.80 ± 0.01 bc
Ferric chloride + AOP	0.498 ± 0.01 e	0.040 ± 0.001 e	1.78 ± 0.01 b	1.82 ± 0.01 b
White WW				
AOP	0.309 ± 0.01 a	0.025 ± 0.003 a	2.56 ± 0.26 a	2.59 ± 0.26 a
DG + AOP	0.359 ± 0.01 b	0.029 ± 0.003 b	2.04 ± 0.20 b	2.07 ± 0.21 b
FA + AOP	0.326 ± 0.01 c	0.026 ± 0.003 a	2.05 ± 0.21 b	2.08 ± 0.21 bcd
DC + AOP	0.456 ± 0.01 d	0.037 ± 0.004 c	2.31 ± 0.23 c	2.35 ± 0.24 ac
TV + AOP	0.357 ± 0.01 b	0.029 ± 0.003 b	2.02 ± 0.20 b	2.05 ± 0.21 b
Rachis + AOP	0.635 ± 0.02 e	0.051 ± 0.005 d	1.22 ± 0.12 d	1.27 ± 0.13
Ferric chloride + AOP	0.432 ± 0.01 f	0.035 ± 0.004 e	2.32 ± 0.23 c	2.35 ± 0.24 ad

that white WW is more sensitive to the oxidation process. Finally, the combined CFD-KPS-photo-Fenton was applied to the treatment of red and white WW, and it is concluded that the combined process decreases the operational cost and is efficient, and the parameters reach the Portuguese legislation for wastewater discharge.

This research showed to be promising in terms of agro-industrial wastewaters treatment, by the combination of natural products with AOPs. However, there are still subjects that can be studied in future works, such as (1) the use of agro-industrial sub-products as natural coagulants, (2) application of invasive and autochthonous plants and (3) assess continuous systems for the treatment of agro-industrial wastewaters with CFD-AOPs.

Credit authors statement

Nuno Jorge: Conceptualization, Writing – original draft, preparation, Methodology, Investigation, Formal analysis, Data curation. **Ana R. Teixeira**: Conceptualization, Resources, Writing – review & editing. **Marco S. Lucas**: Supervision, Validation, Writing – review & editing, Project administration. **José A. Peres**: Supervision, Validation, Writing – review & editing, Project administration.

Funding

The authors are grateful for the financial support of the Project AgriFood XXI, operation n° NORTE-01-0145-FEDER-000041, and to the Fundação para a Ciência e a Tecnologia (FCT) for the financial support provided to CQVR through UIDB/00616/2020. Ana R. Teixeira also thanks the FCT for the financial support provided through the doctoral scholarship UI/BD/150,847/2020.

Declaration of competing interest

The authors declare that they have no known competing financial interests or personal relationships that could have appeared to influence the work reported in this paper.

Data availability

No data was used for the research described in the article.

Acknowledgements

The authors are grateful for the support provided by the Unidade de Microscopia Eletrónica (UME) of UTAD. Open Access funding provided thanks to the CRUE-CSIC agreement with Elsevier and to the Universidade de Vigo/CISUG.

Appendix A. Supplementary data

Supplementary data to this article can be found online at https://doi.org/10.1016/j.jenvman.2022.116819.

References

Amaral-Silva, N., Martins, R.C., Paiva, C., Castro-Silva, S., Quinta-Ferreira, R.M., 2016. A new winery wastewater treatment approach during vintage periods integrating ferric coagulation, Fenton reaction and activated sludge. J. Environ. Chem. Eng. 4, 2207–2215. https://doi.org/10.1016/j.jece.2016.03.044.

Amor, C., Lucas, M.S., Pirra, A.J., Peres, J.A., 2012. Treatment of concentrated fruit juice wastewater by the combination of biological and chemical processes. J. Environ. Sci. Heal. - Part A Toxic/Hazardous Subst. Environ. Eng. 47, 1809–1817. https://doi.org/10.1080/10934529.2012.689244.

Amor, C., Torres-Socías, E. De, Peres, J.A., Maldonado, M.I., Oller, I., Malato, S., Lucas, M.S., 2015. Mature landfill leachate treatment by coagulation/flocculation combined with Fenton and solar photo-Fenton processes. J. Hazard Mater. 286, 261–268. https://doi.org/10.1016/j.jhazmat.2014.12.036.

Amuda, O.S., Amoo, I.A., Ajayi, O.O., 2006. Performance optimization of coagulant/flocculant in the treatment of wastewater from a beverage industry. J. Hazard Mater. 129, 69–72. https://doi.org/10.1016/j.jhazmat.2005.07.078.

APHA, AWWA, WEF, 1999. Standard Methods for the Examination of Water and Wastewater, twentieth ed. American Public Health Association, American Water Works Association, Water Environment Federation.

Baptista, A.T.A., Silva, M.O., Gomes, R.G., Bergamasco, R., Vieira, M.F., Vieira, A.M.S., 2017. Protein fractionation of seeds of Moringa oleifera lam and its application in superficial water treatment. Separ. Purif. Technol. 180, 114–124. https://doi.org/10.1016/j.seppur.2017.02.040.

Barros, V.G. de, Rodrigues, C.S.D., Botello-Suarez, W.A., Duda, R.M., Oliveira, R.A., , de, Silva, E.S. da, Faria, J.L., Boaventura, R.A.R., Madeira, L.M., 2020. Treatment of biodigested coffee processing wastewater using Fenton's oxidation and coagulation/flocculation. Environ. Pollut. 259, 113796 https://doi.org/10.1016/j.envpol.2019.113796.

Beltrán-Heredia, J., Sánchez-Martín, J., Munoz-Serrano, A., Peres, J.A., 2012. Towards overcoming TOC increase in wastewater treated with Moringa oleiferaseed extract. Chem. Eng. J. 188, 40–46. https://doi.org/10.1016/j.cej.2012.02.003.

Benkelberg, H.-J., Warneck, P., 1995. Photodecomposition of iron (III) hydroxo and sulfato complexes in aqueous solution: wavelength dependence of OH and SO4- quantum yields. J. Phys. Chem. 99, 5214–5221. https://doi.org/10.1021/j100014a049.

Boczkaj, G., Fernandes, A., 2017. Wastewater treatment by means of advanced oxidation processes at basic pH conditions: a review. Chem. Eng. J. 320, 608–633. https://doi.org/10.1016/j.cej.2017.03.084.

Boulaadjoul, S., Zemmouri, H., Bendjama, Z., Drouiche, N., 2018. A novel use of Moringa oleifera seed powder in enhancing the primary treatment of paper mill effluent. Chemosphere 206, 142–149. https://doi.org/10.1016/j.chemosphere.2018.04.123.

Braz, R., Pirra, A., Lucas, M.S., Peres, J.A., 2010. Combination of long term aerated storage and chemical coagulation/flocculation to winery wastewater treatment. Desalination 263, 226–232. https://doi.org/10.1016/j.desal.2010.06.063.

Çalık, Ç., Çifçi, D.İ., 2022. Comparison of kinetics and costs of Fenton and photo-Fenton processes used for the treatment of a textile industry wastewater. J. Environ. Manag. 304, 114234 https://doi.org/10.1016/j.jenvman.2021.114234.

Camacho, F.P., Sousa, V.S., Bergamasco, R., Teixeira, M.R., 2017. The use of Moringa oleifera as a natural coagulant in surface water treatment. Chem. Eng. J. 313, 226–237. https://doi.org/10.1016/j.cej.2016.12.031.

Cerdeira, A.L., Duke, S.O., 2006. The current status and environmental impacts of glyphosate-resistant crops: a review. J. Environ. Qual. 35, 1633–1658. https://doi.org/10.2134/jeq2005.0378.

Chen, J., Qian, Y., Liu, H., Huang, T., 2016. Oxidative degradation of diclofenac by thermally activated persulfate: implication for ISCO. Environ. Sci. Pollut. Res. 23, 3824–3833. https://doi.org/10.1007/s11356-015-5630-0.

Chung, C.Y., Selvarajoo, A., Sethu, V., Koyande, A.K., Arputhan, A., Lim, Z.C., 2018. Treatment of palm oil mill effluent (POME) by coagulation flocculation process using peanut – okra and wheat germ – okra. Clean Technol. Environ. Policy 20, 1951–1970. https://doi.org/10.1007/s10098-018-1619-y.

Dbira, S., Bensalah, N., Zagho, M.M., Ennahaoui, M., Bedoui, A., 2019. Oxidative degradation of tannic acid in aqueous solution by UV/S2O82− and UV/H2O2/Fe2+ processes: a comparative study. Appl. Sci. 9, 156. https://doi.org/10.3390/app9010156.

Domínguez, J.R., González, T., García, H.M., Sánchez-Lavado, F., Heredia, J.B. de, 2007. Aluminium sulfate as coagulant for highly polluted cork processing wastewaters: removal of organic matter. J. Hazard Mater. 148, 15–21. https://doi.org/10.1016/j.jhazmat.2007.05.003.

Dükkancı, M., 2018. Sono-photo-Fenton oxidation of bisphenol-A over a LaFeO3 perovskite catalyst. Ultrason. Sonochem. 40, 110–116. https://doi.org/10.1016/j.ultsonch.2017.04.040.

Epold, I., Trapido, M., Dulova, N., 2015. Degradation of levofloxacin in aqueous solutions by Fenton, ferrous ion-activated persulfate and combined Fenton/persulfate systems. Chem. Eng. J. 279, 452–462. https://doi.org/10.1016/j.cej.2015.05.054.

Ganiyu, S.O., Sable, S., El-din, M.G., 2022. Advanced oxidation processes for the degradation of dissolved organics in produced water: a review of process performance, degradation kinetics and pathway. Chem. Eng. J. 429, 132492 https://doi.org/10.1016/j.cej.2021.132492.

Ghernaout, D., Simoussa, A., Alghamdi, A., Ghernaout, B., Elboughdiri, N., Mahjoubi, A., Aichouni, M., El-Wakil, A.E.-A., 2018. Combining lime softening with alum coagulation for hard Ghrib dam water conventional treatment. Int. J. Adv. Appl. Sci. 5, 61–70. https://doi.org/10.21833/ijaas.2018.05.008.

Hilles, A.H., Abu, S.S., Hussein, R.A., El-sebaie, O.D., Arafa, A.I., 2016. Performance of combined sodium persulfate/H2O2 based advanced oxidation process in stabilized land fi ll leachate treatment. J. Environ. Manag. 166, 493–498. https://doi.org/10.1016/j.jenvman.2015.10.051.

Howe, K.J., Hand, D.W., Crittenden, J.C., Trussell, R.R., Tchobanoglous, G., 2012. Principles of Water Treatment. John Wiley & Sons, Inc., New Jersey.

Huie, R.E., Clifton, C.L., Neta, P., 1991. Electron transfer reaction rates and equilibria of the carbonate and sulfate radical anions. Int. J. Radiat. Appl. Instrum. C Radiat. Phys. Chem. 38, 477–481. https://doi.org/10.1016/1359-0197(91)90065-a.

Ince, N.H., Stefan, M.I., Bolton, J.R., 1997. UV/H202 degradation and toxicity reduction of textile azo dyes: remazol black-B , a case study. J. Adv. Oxid. Technol. 2, 442–448. https://doi.org/10.1515/jaots-1997-0312.

Ishak, A.R., Hamid, F.S., Mohamad, S., Tay, K.S., 2018. Stabilized landfill leachate treatment by coagulation-flocculation coupled with UV-based sulfate radical oxidation process. Waste Manag. 76, 575–581. https://doi.org/10.1016/j.wasman.2018.02.047.

Iwahashi, M., Tachibana, Y., Ohta, Y., 1982. Soil Science and Plant Nutrition Accumulation of calcium, magnesium, potassium and sodium with growth of individual leaves, petioles and stems of cucumber plants. Soil Sci. Plant Nutr. 28, 441–449. https://doi.org/10.1080/00380768.1982.10432384.

Jorge, N., Teixeira, A.R., Guimarães, V., Lucas, M.S., Peres, J.A., 2022a. Treatment of winery wastewater with a combination of adsorption and thermocatalytic processes. Processes 10, 75. https://doi.org/10.3390/pr10010075.

Jorge, N., Teixeira, A.R., Lucas, M.S., Peres, J.A., 2022b. Agro-industrial wastewater treatment with Acacia dealbata coagulation/flocculation and photo-fenton-based processes. Recycling 7, 54. https://doi.org/10.3390/recycling7040054.

Jorge, N., Teixeira, A.R., Matos, C.C., Lucas, M.S., Peres, J.A., 2021. Combination of coagulation–flocculation–decantation and ozonation processes for winery wastewater treatment. Int. J. Environ. Res. Publ. Health 18, 8882. https://doi.org/10.3390/ijerph18168882.

Khan, N.A., Husain, A., Tiwari, P., Zubair, M., Naushad, M., 2021. New insights into the integrated application of Fenton-based oxidation processes for the treatment of pharmaceutical wastewater. J. Water Proc. Eng. 44, 102440 https://doi.org/10.1016/j.jwpe.2021.102440.

Khataee, A., Aleboyeh, H., Sheydaei, M., Aleboyeh, A., 2016. Comprehensive monitoring of the performance of homogenous and heterogeneous UV/H2O2/S2O82-/Fe2+ processes in mineralization of Acid Red 73. Res. Chem. Intermed. 42, 571–580. https://doi.org/10.1007/s11164-015-2042-1.

Ko, S., Crimi, M., Marvin, B.K., Holmes, V., Huling, S.G., 2012. Comparative study on oxidative treatments of NAPL containing chlorinated ethanes and ethenes using hydrogen peroxide and persulfate in soils. J. Environ. Manag. 108, 42–48. https://doi.org/10.1016/j.jenvman.2012.04.034.

Kushwaha, A.K., Gupta, N., Chattopadhyaya, M.C., 2014. Removal of cationic methylene blue and malachite green dyes from aqueous solution by waste materials of Daucus carota. J. Saudi Chem. Soc. 18, 200–207. https://doi.org/10.1016/j.jscs.2011.06.011.

Lak, M.G., Sabour, M.R., Ghafari, E., Amiri, A., 2018. Energy consumption and relative efficiency improvement of Photo-Fenton–Optimization by RSM for landfill leachate treatment, a case study. Waste Manag. 79, 58–70. https://doi.org/10.1016/j.wasman.2018.07.029.

Li, M., Yang, X., Wang, D., Yuan, J., 2017. Enhanced oxidation of erythromycin by persulfate activated iron powder – H2O2 system: role of the surface Fe species and synergistic effect of hydroxyl and sulfate radicals. Chem. Eng. J. 317, 103–111. https://doi.org/10.1016/j.cej.2016.12.126.

Lin, W., Liu, X., Ding, A., Ngo, H.H., Zhang, R., Nan, J., Ma, J., Li, G., 2022. Advanced oxidation processes (AOPs)-based sludge conditioning for enhanced sludge dewatering and micropollutants removal: a critical review. J. Water Proc. Eng. 45, 102468 https://doi.org/10.1016/j.jwpe.2021.102468.

Lucas, M.S., Peres, J.A., 2009. Removal of COD from olive mill wastewater by Fenton's reagent: kinetic study. J. Hazard Mater. 168, 1253–1259. https://doi.org/10.1016/j.jhazmat.2009.03.002.

Lucas, M.S., Peres, J.A., 2007. Degradation of Reactive Black 5 by Fenton/UV-C and ferrioxalate/H2O2/solar light processes. Dyes Pigments 74, 622–629. https://doi.org/10.1016/j.dyepig.2006.04.005.

Lucas, M.S., Peres, J.A., Li, G., 2010. Treatment of winery wastewater by ozone-based advanced oxidation processes (O3, O3/UV and O3/UV/H2O2) in a pilot-scale bubble column reactor and process economics. Separ. Purif. Technol. 72, 235–241. https://doi.org/10.1016/j.seppur.2010.01.016.

Mageshkumar, M., Karthikeyan, R., 2016. Modelling the kinetics of coagulation process for tannery industry effluent treatment using Moringa oleifera seeds protein. Desalination Water Treat. 57, 14954–14964. https://doi.org/10.1080/19443994.2015.1070294.

Malandra, L., Wolfaardt, G., Zietsman, A., Viljoen-bloom, M., 2003. Microbiology of a biological contactor for winery wastewater treatment. Water Res. 37, 4125–4134. https://doi.org/10.1016/S0043-1354(03)00339-7.

Marañón, E., Castrillón, L., Fernández-Nava, Y., Fernández-Méndez, A., 2015. Colour , turbidity and COD removal from old landfill leachate by coagulation-flocculation treatment. Waste Manag. Res. 28, 731–737. https://doi.org/10.1177/0734242X09352504.

Peres, J.A., de Heredia, J.B., Domınguez, J.R., 2004. Integrated Fenton's reagent—coagulation/flocculation process for the treatment of cork processing wastewaters. J. Hazard Mater. 107, 115–121. https://doi.org/10.1016/j.jhazmat.2003.09.012.

Perez, M., Torrades, F., Garcıa Hortal, J.A., Domènech, X., Peral, J., 2002. Removal of organic contaminants in paper pulp treatment effluents under Fenton and photo-Fenton conditions. Appl. Catal. B Environ. 36, 63–74. https://doi.org/10.1002/jctb.610.

Petruccioli, M., Cardoso Duarte, J., Eusebio, A., Federici, F., 2002. Aerobic treatment of winery wastewater using a jet-loop activated sludge reactor. Process Biochem. 37, 821–829. https://doi.org/10.1016/S0032-9592(01)00280-1.

Prozil, S.O., Evtuguin, D.V., Silva, A.M., Lopes, L.P., 2014. Structural characterization of lignin from grape stalks (Vitis vinifera L.). J. Agric. Food Chem. 62, 5420–5428. https://doi.org/10.1021/jf502267s.

Rana, R., Herz, K., Bruelheide, H., Dietz, S., Haider, S., 2018. Leaf Attenuated Total Reflection Fourier Transform Infrared (ATR-FTIR) biochemical profile of grassland plant species related to land-use intensity. Ecol. Indicat. 84, 803–810. https://doi.org/10.1016/j.ecolind.2017.09.047.

Rifi, S.K., Souabi, S., Fels, L. El, Driouich, A., Nassri, I., Haddaji, C., Hafidi, M., 2022. Optimization of coagulation process for treatment of olive oil mill wastewater using Moringa oleifera as a natural coagulant, CCD combined with RSM for treatment optimization. Process Saf. Environ. Protect. 162, 406–418. https://doi.org/10.1016/j.psep.2022.04.010.

Rodríguez-Chueca, J., Amor, C., Mota, J., Lucas, M.S., Peres, J.A., 2017. Oxidation of winery wastewater by sulphate radicals: catalytic and solar photocatalytic activations. Environ. Sci. Pollut. Res. 24, 22414–22426. https://doi.org/10.1007/s11356-017-9896-2.

Shu, H., Huang, S., Tsai, M., 2016. Comparative study of acid blue 113 wastewater degradation and mineralization by UV/persulfate and UV/Oxone processes. Desalination Water Treat. 57, 29517–29530. https://doi.org/10.1080/19443994.2016.1172031.

Singleton, V.L., Rossi, J.A., 1965. Colorimetry of total phenolics with phosphomolybdic-phosphotungstic acid reagents. Am. J. Enol. Vitic. 16, 144–158.

Teixeira, A.R., Jorge, N., Fernandes, J.R., Lucas, M.S., Peres, J.A., 2022. Textile dye removal by Acacia dealbata link. Pollen adsorption combined with UV-A/NTA/Fenton process. Top. Catal. 1–17 https://doi.org/10.1007/s11244-022-01655-w.

Thommes, M., Kaneko, K., Neimark, A.V., Olivier, J.P., Rodriguez-Reinoso, F., Rouquerol, J., Sing, K.S., 2015. Physisorption of gases, with special reference to the evaluation of surface area and pore size distribution (IUPAC Technical Report). Pure Appl. Chem. 87, 1051–1069. https://doi.org/10.1515/ci-2016-0119.

Vunain, E., Mike, P., Mpeketula, G., Monjerezi, M., Etale, A., 2019. Evaluation of coagulating efficiency and water borne pathogens reduction capacity of Moringa oleifera seed powder for treatment of domestic wastewater from Zomba, Malawi. J. Environ. Chem. Eng. 7, 103118 https://doi.org/10.1016/j.jece.2019.103118.

Wang, Y.R., Chu, W., 2012. Photo-assisted degradation of 2,4,5-trichlorophenoxyacetic acid by Fe(II)-catalyzed activation of Oxone process: the role of UV irradiation, reaction mechanism and mineralization. Appl. Catal. B Environ. 123–124, 151–161. https://doi.org/10.1016/j.apcatb.2012.04.031.

Welz, P.J., Holtman, G., Haldenwang, R., le Roes-Hill, M., 2016. Characterisation of winery wastewater from continuous flow settling basins and waste stabilisation ponds over the course of 1 year: implications for biological wastewater treatment and land application. Water Sci. Technol. 74, 2036–2050. https://doi.org/10.2166/wst.2016.226.

Xu, X., Yang, Y., Jia, Y., Lian, X., Zhang, Y., Feng, F., Liu, Q., Xi, B., Jiang, Y., 2019. Heterogeneous catalytic degradation of 2, 4-dinitrotoluene by the combined persulfate and hydrogen peroxide activated by the as-synthesized Fe-Mn binary oxides. Chem. Eng. J. 374, 776–786. https://doi.org/10.1016/j.cej.2019.05.138.

Yan, N., Liu, F., Huang, W., 2013. Interaction of oxidants in siderite catalyzed hydrogen peroxide and persulfate system using trichloroethylene as a target contaminant. Chem. Eng. J. 219, 149–154. https://doi.org/10.1016/j.cej.2012.12.072.

Yin, X.L., Jiang, L., Song, N.H., Yang, H., 2008. Toxic reactivity of wheat (Triticum aestivum) plants to herbicide isoproturon. J. Agric. Food Chem. 56, 4825–4831. https://doi.org/10.1021/jf800795v.

Zimmermann, B., Bağcıoğlu, M., Tafinstseva, V., Kohler, A., Ohlson, M., Fjellheim, S., 2017. A high-throughput FTIR spectroscopy approach to assess adaptive variation in

the chemical composition of pollen. Ecol. Evol. 7, 10839–10849. https://doi.org/10.1002/ece3.3619.